Hyperactivation of sympathetic nerves drives depletion of melanocyte stem cells

Stress-Mediated Hyperactivation of Sympathetic Nerves Drives Melanocyte Stem Cell Depletion

Bing Zhang[1], Sai Ma[1,2,9], Inbal Rachmin[3], Megan He[1,4], Pankaj Baral[5], Sekyu Choi[1], William Gonçalves[6], Yulia Shwartz[1], Eva Maria Fast[1,7], Yiqun Su[3], Leonard I. Zon[1,7,8], Aviv Regev[2,8,9], Jason D. Buenrostro[1], Thiago Mattar Cunha[5,10], Isaac M. Chiu[5], David E. Fisher[3], Ya-Chieh Hsu[1*]

[1]Department of Stem Cell and Regenerative Biology, Harvard University and Harvard Stem Cell Institute, Cambridge, MA, USA.

[2]Broad Institute of MIT and Harvard, Cambridge, MA, USA

[3]Cutaneous Biology Research Center, Department of Dermatology, Massachusetts General Hospital, Harvard Medical School, Charlestown, MA, USA

[4]Molecules, Cells, and Organisms PhD Program, Department of Molecular and Cellular Biology, Harvard University, Cambridge, Massachusetts.

[5]Department of Microbiology and Immunobiology, Division of Immunology, Harvard Medical School, Boston, MA, USA

[6]Graduate Program in Cellular Biology, Institute of Biological Science, Federal University of Minas Gerais, Belo Horizonte, MG, Brazil

[7]Stem Cell Program and Division of Pediatric Hematology/Oncology, Boston Children's Hospital, Dana-Farber Cancer Institute, Harvard Medical School, Boston, MA, USA

[8]Howard Hughes Medical Institute, Chevy Chase, MD, USA

[9]Department of Biology and Koch Institute, Massachusetts Institute of Technology, Cambridge, MA, USA

[10]Center for Research in Inflammatory Diseases (CRID), Department of Pharmacology, Ribeirão Preto Medical School, University of São Paulo, Av. Bandeirantes, 3900, Ribeirão Preto, SP, Brazil.

[*]Correspondence to:
Ya-Chieh Hsu, PhD (**Lead Contact**)
yachieh_hsu@harvard.edu

Summary

Stress is an out of the norm state caused by emotional or physical insults. While chronic stress is considered harmful, acute stress is thought to cause transient and reversible changes essential for fight or flight. Stress has been anecdotally associated with hair greying, but scientific evidence linking the two is scant. Here, using mouse stress models, we found that acute stress leads to hair greying through rapid depletion of melanocyte stem cells (MeSCs). Combining adrenalectomy, denervation, chemogenetics, cell ablation, and MeSC-specific adrenergic receptor knockout, we found that stress-induced MeSC loss is independent of the immune attack or adrenal hormones. Instead, hair greying results from activation of the sympathetic nervous system that innervates the MeSC niche. Upon stress, sympathetic nerve activation leads to burst release of the neurotransmitter norepinephrine, which acts directly on MeSCs. Norepinephrine drives quiescent MeSCs to proliferate rapidly, followed by migration and differentiation, leading to their permanent depletion from the niche. Transient suppression of MeSC proliferation with topical application of cell cycle inhibitors rescues stress-induced hair greying. Our studies demonstrate that stress-induced neuronal activity can be an upstream trigger that forces stem cells out of quiescence, and suggest that acute stress stimuli can be more detrimental than anticipated by causing rapid and irreversible loss of somatic stem cells.

Introduction

Stress affects people of all ages, genders, and occupations, and is thought to be a risk factor for numerous diseases and disorders. Despite their profound impact, whether and how external stressors lead to tissue changes, and if stress-related changes occur at the level of somatic stem cells, is not well understood. Establishing the mechanisms of these stress-induced tissue changes is crucial to understand if and how psychological states shape stem cell behaviours and tissue functions. Such mechanistic insights will also identify genes and pathways that may be useful for

reducing or reverting the undesirable effects of stress on stem cell function and tissue homeostasis.

Tales of famous historical figures have associated hair greying (formation of unpigmented hairs) with stress. In ancient China, general Wu Zixu's hair turned white within days when he attempted to escape tight border controls under an execution order. Similarly, the hair of Queen Marie Antoinette of France turned white shortly after her capture during the French Revolution. Since then, the "Marie Antoinette Syndrome" has been used to describe the condition in which a person's hair turns white within a short time[1]. Still, whether stress indeed triggers hair greying remains an open question.

Melanocyte stem cells (MeSCs) play a key role in hair pigmentation and contribute to the formation of melanoma[2–6]. MeSCs are intermingled with the hair follicle stem cells (HFSCs) in the bulge and the hair germ[6,7]. The hair follicle cycles between growth (anagen), degeneration (catagen), and rest (telogen). HFSCs and MeSCs are in strict quiescence during most of the hair cycle except during early anagen, when both HFSCs and MeSCs are activated concurrently to regenerate a pigmented hair[8,9]. Activation of HFSCs produces a new hair follicle. Activation of MeSCs generates differentiated melanocytes that migrate downward to the hair bulb, while MeSCs remain at the upper Outer Root Sheath (ORS) beneath the bulge. At the hair bulb, differentiated melanocytes synthesize melanin which colours the newly regenerated hair from the root. At catagen, mature melanocytes are destroyed, the process sparing only the MeSCs that will initiate another round of melanogenesis in the next hair cycle (Extended Data Fig.1a)[10,11]. The stereotypic behaviour of MeSCs and differentiated melanocytes within a hair cycle, and the visible nature of hair colour, makes the melanocyte lineage an accessible model to investigate how stress influences somatic stem cells and tissue regeneration.

Here, we investigated the effect of stress on MeSCs and melanocyte lineages. By testing the impact of several established stressors, we found that stress indeed leads to hair greying in rodents. Although stress elevates systemic levels of stress hormones and catecholamines derived

from the adrenal glands, we found that adrenal glands are, surprisingly, dispensable for stress-induced hair greying. Instead, stress triggers a burst activation of sympathetic nerves, which secrete norepinephrine, a neurotransmitter that drives MeSCs out of quiescence and leads to their depletion. Deleting the receptor for norepinephrine or blocking MeSC proliferation alleviates the detrimental effect of stress on MeSCs. Our findings illustrate an example in which somatic stem cell function is directly influenced by the overall physiological state of the organism. Moreover, we illustrate an unexpected cross-system interaction in which burst elevation of neuronal activity has the potency to rapidly and permanently deplete a non-neuronal stem cell population. Lastly, our findings also suggest ways in which the stem cell depletion can be prevented, even in the face of acute or severe physiological challenges.

Results

Hair greying occurs when mice are subjected to diverse stressors

To examine whether psychological or physical stressors can promote hair greying, we applied three independent approaches to model stress in black coat colour C57/BL6 mice: restraint stress[12,13], chronic unpredictable stress[14–17], and nociception-induced stress via injection of resiniferatoxin (RTX, a capsaicin analogue)[18–20]. All three procedures led to increased numbers of unpigmented white hairs over time. Restraint stress and chronic unpredictable stress led to significant hair greying after 3-5 rounds of hair cycles. Nociception-induced stress produced the most pronounced and rapid effect, leading to formation of many unpigmented white hairs as soon as the following hair cycle (Fig. 1a, b, Extended Data Fig. 1b, c).

Physical or psychological stressors are known to trigger a hormonal cascade that starts from the hypothalamus, proceeds through the pituitary gland, and eventually reaches the adrenal glands to promote the release of stress hormones and catecholamines into the bloodstream (the HPA axis, Fig. 1c)[21–23]. To verify that the different stressors we employed were effective in eliciting stress responses, we measured levels of corticosterone (cortisol equivalent in rodents, a classical stress hormone) and norepinephrine (a catecholamine) in the blood of control and stressed mice.

Liquid chromatography with tandem mass spectrometry (LC-MS-MS) analyses revealed an increase in both corticosterone and norepinephrine in mice subjected to stressors (Fig. 1d, Extended Data Fig. 1d), suggesting that classical stress responses were induced successfully with these different procedures.

RTX induces pain by activating peripheral nociceptive sensory neurons[24–26]. Blocking the ability of an animal to feel pain with buprenorphine (a broad spectrum, long-acting opioid analgesic) prevents the increases of corticosterone and norepinephrine in the blood after RTX injection, suggesting that blocking pain sensation alleviates the physiological stress responses induced by RTX (Fig. 1d). Interestingly, animals injected with both RTX and analgesia did not display stress responses, and also did not develop white hairs (Fig. 1e). These data reveal an association between stress responses and hair greying, and suggest that premature hair greying can occur when the mice are subjected to stressors. Because the effect of nociception induction on hair greying is the strongest and most rapid among the three stressors tested, we focused on RTX injection as our primary stressor for most of the remaining studies.

Stress leads to loss of MeSCs

Loss of hair pigmentation can be due to defects in the melanin synthesis pathway[27–30], loss of differentiated melanocytes[31], or problems in MeSC maintenance[32]. To understand how stress impacts the melanocyte lineage, we injected RTX into mice that were in anagen, when both the MeSCs and differentiated melanocytes were present but located within distinct compartments—MeSCs are at the upper ORS region close to the bulge, while differentiated melanocytes are down within the hair bulb (Fig. 1f, Extended data Fig. 1a). Upon RTX injection, TRP2+ MeSCs were lost from the upper ORS within 5 days, while the differentiated melanocytes remained unperturbed (Fig. 1f, left). These differentiated melanocytes still generated pigment for the new hair, and the hair coat remained black at this stage (Extended data Fig. 2a). When the hair follicles in the RTX-injected animals entered catagen and telogen, no MeSCs remained (Fig. 1f, middle). Subsequently, when the next round of anagen initiated, differentiated melanocytes

could not be produced, and unpigmented hair was formed (Fig. 1f, right). Similar effects on MeSC loss were observed if RTX was injected during telogen (Extended data Fig. 2b). These results suggest that the MeSCs are exquisitely sensitive to RTX-induced stress, while the differentiated melanocytes or melanin synthesis pathways are not directly affected. MeSC numbers were also lost or significantly reduced in mice subjected to restraint stress or chronic unpredictable stress (Extended data Fig. 2c). Since the effect of stress was to deplete MeSCs, the loss of hair pigmentation in all three stress-inducing conditions was permanent (Extended data Fig. 2d). Collectively, these data indicate that stress leads to loss of MeSCs.

Norepinephrine drives hair greying by acting on MeSCs directly

Next, we aimed to understand how stress transmits signals to the periphery to alter MeSCs biology. Immune attack has been postulated to be the underlying cause of the Marie Antoinette syndrome[33,34], and stress is thought to lead to changes in immune cell composition and immune responses[35]. To test the involvement of the immune system, we injected RTX into Rag1 mutant mice, which lack both T cells and B cells, and into CD11b-DTR mice, in which myeloid lineages had been ablated by diphtheria toxin (DT). Injection of RTX into these immune-deficient mice still led to white hair formation, suggesting that RTX-induced hair greying is independent of adaptive immune cell- or myeloid immune cell-mediated attack (Fig. 2a, b, Extended Data Fig. 3a, b).

Because we found that nociception and other stressors led to elevated corticosterone and norepinephrine in the blood, we asked if any of these stress-induced circulating factors played a role in RTX-induced MeSC loss (Fig. 2a). Our RNA sequencing (RNA-seq) data suggested that MeSCs express the glucocorticoid receptor (GR, a receptor for corticosterone) as well as the β2 adrenergic receptor (*Adrb2*, a receptor for norepinephrine) (Fig. 2c). To determine if GR mediates the effects of stress on MeSCs, we depleted GR in MeSCs specifically using Tyr-CreER at telogen, an inducible CreER expressed in MeSCs[3,4,9,36]. RTX injection into Tyr-CreER; GR fl/fl animals still resulted in white hair formation, suggesting that stress-induced hair greying is independent of whether MeSCs can receive the stress hormone corticosterone or not (Fig. 2d). In marked

contrast, when we depleted *Adrb2* from MeSCs specifically using the same Tyr-CreER line (*Adrb2* cKO), white hairs failed to form following RTX injection (Fig. 2e). In addition, when Adrb2 is depleted from hair follicle stem cells that share the same niche with MeSCs, RTX injection still led to hair greying (Extended Data Fig. 3c). Altogether, these data suggest that norepinephrine signalling through ADRB2 is an essential mediator of stress-induced hair greying. Moreover, our MeSC-specific *Adrb2* vs. HFSC-specific *Adrb2* knockout also demonstrate that norepinephrine acts on MeSCs directly, not on the HFSCs located in the same niche.

To test if elevated norepinephrine by itself was sufficient to cause hair greying without any added stressor, we introduced norepinephrine into a small region of the skin via intradermal injection. Local norepinephrine injection was sufficient to promote hair greying in the injected area in the absence of stress (Fig. 2f). Altogether, our data demonstrate that while immune cells and corticosterone are dispensable, localized norepinephrine signalling appears to be both necessary and sufficient in mediating the impact of stress on hair greying.

Activation of the sympathetic nervous system leads to hair greying

Since the adrenal gland is thought to be a major source of norepinephrine under stress, to determine if adrenal gland-derived norepinephrine mediates stress-induced hair greying, we performed complete adrenalectomy by surgical removal of both adrenal glands. Adrenalectomy significantly reduced the levels of corticosterone and norepinephrine in the bloodstream in the RTX-injected animals (Fig. 2g). These results confirmed the efficacy of surgery, and also established that the adrenal glands are indeed responsible for the elevated levels of corticosterone and norepinephrine in the blood under stress. Yet, to our surprise, injection of RTX into adrenalectomized mice still resulted in hair greying, suggesting that RTX-induced hair greying is independent of hormones or catecholamines secreted from the adrenal glands (Fig. 2h). These results prompted us to explore additional sources of norepinephrine that might be responsible for hair greying.

One possible alternative source of norepinephrine is the sympathetic nervous system. The cell bodies of sympathetic nerves are located in the sympathetic ganglia, and sympathetic axons innervate all organs to regulate diverse physiological responses including the skin[37–41] (Fig. 3a). In response to stress, sympathetic nerves are highly activated to mediate fight or flight responses through secretion of norepinephrine from peripheral nerve terminals[41]. In the skin, sympathetic nerves terminate close to the bulge where the MeSCs reside, suggesting the potential for neurotransmitters secreted from sympathetic nerves to reach MeSCs directly (Fig. 3a).

To determine if sympathetic nerves are indeed activated following RTX injection, we examined levels of C-FOS, an immediate early transcription factor for nerve activation[42,43]. Robust C-FOS expression was detected in the sympathetic neuronal cell bodies located within the sympathetic chain ganglia within 1 hour after RTX injection, peaking around 2-4 hours, and diminishing after 24 hours, suggesting that RTX injection led to burst activation of the sympathetic nervous system (Fig. 3b, Extended data Fig. 4). Moreover, when RTX was injected together with analgesic blockade using buprenorphine, sympathetic neurons failed to show C-FOS induction (Fig. 3b, right). Together, these data suggest that sympathetic nervous system becomes highly activated following nociception-induced stress.

To test if activation of sympathetic nerves is responsible for MeSC loss and hair greying, we ablated sympathetic nerves using 6-hydroxy dopamine (6-OHDA), a selective neurotoxin for sympathetic nerves[44]. Sympathectomy blocked RTX-induced hair greying and MeSC loss effectively (Fig. 3c), suggesting that sympathetic nerves indeed mediate stress-related hair greying. In addition, guanethidine, a chemical that specifically blocks norepinephrine release from the sympathetic nerve terminals without affecting the nerve fibres[45–47], suppressed hair greying and MeSC loss upon RTX injection (Fig. 3d). Collectively, these data suggest that norepinephrine secreted from the sympathetic nerve terminals mediates the effect of stress on MeSCs.

To further determine if sympathetic nerve activation in the absence of any stressors was sufficient to drive MeSC loss, we took a chemogenetic approach using the Designer Receptor

Exclusively Activated by Designer Drug (DREADD) system[48,49]. We generated TH-CreER; CAG-LSL-DREADD; Rosa-LSL-mT/mG mice. TH-CreER drives DREADD expression in the sympathetic nerves, which allowed us to activate sympathetic nerves artificially with Clozapine N-Oxide (CNO, Fig. 3e). Sympathetic nerve activation with the DREADD system led to loss of MeSCs locally when CNO was injected intradermally to activate sympathetic nerves that innervate the hair follicles (Fig. 3f). Moreover, when TH-CreER was activated in a mosaic fashion by low dose tamoxifen, intradermal CNO injection resulted in to MeSC loss only in hair follicles innervated by DREADD positive nerve fibres (recognizable by their membrane GFP expression, Fig. 3g). These data suggest that sympathetic nerve activation in the absence of stressors is sufficient to drive MeSC loss. Our functional manipulation of the sympathetic nervous system, together with our MeSC-specific *Adrb2* knockout data (Fig. 2e), suggest that elevated norepinephrine secreted from the sympathetic nerve terminals drives MeSC depletion.

MeSCs lose quiescence and enter a rapid proliferating state under stress

To understand changes in MeSCs after stress stimuli that might account for their loss, we examined changes of MeSCs upon RTX or norepinephrine injection (Fig. 4a). Since MeSCs were depleted from their niche in the bulge within 5 days after RTX injection (Fig. 1f), we focused on the early timepoints before MeSC depletion. We first tested the possibility that MeSCs were depleted through cell death. Immunofluorescence failed to detect active caspase-3 or TUNEL signals before MeSCs were depleted from the niche, suggesting that apoptotic cell death is not a major contributor of MeSC loss under stress (Fig. 4b, Extended data Fig. 5). Moreover, RTX injection into RIP3K mutant mice lacking a key kinase required for necrosis still developed white hairs, suggesting that necrosis is also not a major mediator of MeSC loss under stress (Fig. 4c). Radiation has been shown to cause DNA damage in MeSCs, leading to their direct differentiation within the niche and subsequent hair greying[32]. However, we failed to detect gamma-H2AX foci (a hallmark of DNA damage) in MeSCs following RTX treatment or norepinephrine injection, suggesting that MeSCs are also not depleted through DNA damage under stress (Fig. 4d).

Quiescence is a key feature for many somatic stem cells[50–56]. Loss of quiescence leads to stem cell exhaustion in a wide variety of systems including the hematopoietic system and skeletal muscles, and has been postulated to be the reasons driving MeSC loss in *Bcl2* mutants[57–60]. MeSCs are maintained in a strict quiescent state except during anagen onset, when a small number of MeSCs proliferate transiently to generate differentiated progeny[9,60]. To examine if stress alters the quiescent state of MeSCs, we injected RTX or norepinephrine into mice that had entered full anagen, when MeSCs are normally quiescent. We saw a dramatic increase in the number of proliferating MeSCs one day after RTX or norepinephrine injection— almost all MeSCs became positive for Phospho-Histone H3, an M phase marker (Fig. 4e). The number of proliferating MeSCs upon stress stimuli was substantially more than what was seen in anagen onset, the only stage when MeSCs normally proliferate[2,6]. These data suggest that MeSCs are indeed driven out of quiescence and into a rapid proliferative state under the influence of norepinephrine.

To monitor changes occurring in MeSCs following stress, we crossed Tyr-CreER with Rosa-mT/mG mice, which allowed us to trace MeSCs by membrane GFP staining (Fig. 4f). Consistent with the observation that MeSCs become proliferative in response to stress, we saw a transient increase in GFP positive cells shortly after RTX injection (Fig. 4f, FACS quantified in Fig. 4g, Extended data Fig. 6). Following this initial phase of proliferation and expansion, many GFP positive cells began to exhibit striking dendritic branching, characteristic of differentiated MeSCs (Fig. 4f, D2). They also began to depart from the bulge niche—some migrated downwards along the hair follicles, and some migrated out into dermis or epidermis (Fig. 4f, D3). Brightfield microscopy revealed that these GFP+ cells with dendritic morphology carried pigments, suggesting that they had indeed acquired differentiation features (Fig. 4h) and similar to the ectopic pigmentation seen in age-related or DNA-damage induced MeSC differentiation[32,59]. By Day 3, many of these GFP+ cells had migrated out from the bulge, and by Day 4, many hair follicles had lost all GFP+ cells in the bulge region. Collectively, these data suggest that after

stress stimuli, MeSCs first undergo rapid proliferation followed by differentiation and migration, leading to their rapid loss in the niche (Fig. 4i).

Transcriptome analyses suggest that MeSCs exit quiescence and become committed to differentiation following stress

To discover the molecular mechanisms that might account for MeSC loss, we conducted RNA-seq using FACS-purified MeSCs from control and RTX-treated animals. To capture gene changes that might drive phenotypic changes, we isolated MeSCs by flow cytometry 12 hours after RTX injection, before MeSCs showed clear phenotypic differences (Fig. 5a). Independent replicates of the same condition were similar, allowing us to identify molecular signatures that were differentially expressed between MeSCs isolated from control and stressed animals (Extended data Fig. 7a, b). Moreover, examination of gene counts of marker genes for several epithelial and dermal cell types confirmed that we had successfully enriched for MeSCs (Extended data Fig. 7c). To uncover major molecular changes, we conducted Gene Ontology (GO) enrichment analysis (Fig. 5b). We also curated a list of genes based on published literature on MeSC proliferation and differentiation (Fig. 5c). In addition, we utilized a list of gene signatures previously denoted for cell cycle entry to assess if cell cycle genes are differ at the transcriptional level between control and stressed MeSCs (Extended data Fig.7c)[61–63]. Besides RNAseq, we also verified some of these key changes independently using quantitative RT-PCR (qRT-PCR) (Fig. 5d). From these analyses, we found that several key cell cycle regulators were up-regulated in MeSCs from stressed animals, in particular Cyclin-dependent kinase 2 (*Cdk2*), a key promoter of G1 to S transition[64]. Receptors for signals that promote MeSC proliferation and differentiation, including *c-Kit* and *Mc1r*, were also up-regulated. Lastly, genes involved in melanogenesis, including *Mitf*, *Tyrp1*, *Tyr*, *Oca2*, and *Pmel*, were up-regulated (Fig. 5c, d). Collectively, these data suggest that under RTX-induced stress, MeSCs are driven out of quiescence, lose their stem cell characters, and become committed towards differentiation by upregulating proliferation and differentiation programs.

Having identified the impact of stress on mouse MeSCs, we next wanted to explore if stress can impact human melanocytes through similar mechanisms. For this, we asked if norepinephrine exposure alone might cause similar changes in human melanocytes. For this, we added norepinephrine to primary cultures of human melanocytes isolated from three independent donors. Similar to the results in mice, qRT-PCR analyses showed that norepinephrine led to a rapid and potent induction of *Cdk2*, as well as to expression of melanocyte differentiation genes like *Mitf* and *Tyr* (Fig. 5e). These data suggest that norepinephrine can elicit similar responses in both human and mouse melanocyte lineages.

Inhibition of proliferation prevents MeSC loss and hair greying under stress

Since MeSCs lose their quiescence rapidly upon stress, we asked if transient suppression of proliferation early in the stress response might prevent their depletion. For this, we injected RTX into the animals at full anagen, and applied CDK inhibitors AT7519 or Flavopiridol topically to suppress proliferation transiently until 48 hours post RTX injection[65,66]. 5-7 days post RTX injection, the MeSCs in RTX-injected animals were depleted as expected. By contrast, the MeSCs in RTX-injected animals treated with CDK inhibitors were preserved in the niche (Fig. 5f). These preserved MeSCs displayed undifferentiated morphology. Moreover, ectopic differentiation and migration of MeSCs caused by RTX injection were also suppressed. These results suggest that if MeSCs can be kept in quiescence under stress, MeSCs don't undergo differentiation or migration and can be maintained in the niche. These preserved MeSCs were also functional, as the newly regenerated hairs in the subsequent rounds of hair cycle in these RTX-injected animals treated with CDK inhibitors displayed normal pigmentation (Fig. 5g). Similar suppression effects on MeSC depletion and hair greying were also observed when we overexpressed the CDK inhibitor P27 *in vivo* to block cell proliferation (Fig. 5h, i)[67,68]. Collectively, these data suggest that loss of quiescence is a key contributor to MeSC depletion upon stress, and that suppression of MeSC proliferation is sufficient to prevent their loss.

Discussion

Stress is often thought to be harmful when lasting for a prolonged period of time, through gradual and accumulated long-term changes. In an acute stress situation, transient elevation of catecholamines is critical to eliciting the “fight or flight” response essential for survival. Here, we illustrate an example in which a somatic stem cell population is depleted rapidly and permanently through the action of norepinephrine, a known trigger of the fight or flight response. Our findings suggest that acute stress stimuli can cause non-reversible changes at the level of stem cells, resulting in permanent damage in tissue regeneration. Quiescence has been thought to be a critical feature of stem cell maintenance[10,57,51,52]. Our findings suggest that stress stimuli provide an upstream trigger capable of driving stem cells out of their quiescent state. Although MeSCs also differentiate and migrate out from the niche following the initial proliferative phase, the striking rescue effects of CDK inhibitors demonstrate that MeSC proliferation acts upstream of differentiation and migration upon stress stimulation. These results suggest that loss of quiescence is a crucial mechanism for stress-induced MeSC loss.

The adrenal glands are often thought to be the central regulator of stress responses. Interestingly, we found that while the adrenal glands indeed regulate the levels of stress hormones and catecholamines in the blood, they are dispensable for changes we observed in MeSCs under stress. Our findings support the emerging theme that the sympathetic nervous system not only regulates our body physiology (such as heart rate and blood pressure), but also influences diverse process in development and tissue maintenance[40,69,70]. Sympathetic nerves have also been shown to regulate hematopoietic stem cells, but do so indirectly through innervating the mesenchymal tissues and influencing cytokine expression in the bone marrow stroma[14,38,71,72]. Here, in contrast, we found that sympathetic nerves control MeSCs directly through the neurotransmitter norepinephrine. Since sympathetic nerves innervate essentially all organs, we postulated that acute stress might have a broad impact on many tissues either directly or indirectly through the sympathetic nervous system.

The connection we observed here between the nervous system and pigment producing cells is likely conserved during evolution. Cephalopods like squid, octopus, or cuttlefish have sophisticated colouration systems that allow them to change skin colour instantly for camouflage or communication. It is thought that neuronal activities control their pigment producing cells (chromatophores) directly, allowing rapid changes in colour to occur in response to predators or threats[73,74]. In zebrafish, epinephrine treatment caused rapid but reversible changes in melanin distribution[75,76]. In mammals, pigmentation remains as a first line of defence against UV irradiation. Upon UV-irradiation, keratinocytes secrete melanocyte-stimulating hormone that binds to MC1R on melanocytes to promote differentiation via up-regulation of MITF[77,78]. It is possible that the sympathetic nervous system provides another layer of modulation. Interaction between nerves and MeSCs might allow MeSC activity to be fine-tuned in response to external stimuli such as bright sun light or seasonal changes, which would be consistent with the observation that sympathetic nerve activity is elevated upon stimulation with light[79,80]. This nerve-MeSC connection may facilitate production of differentiated melanocytes and migration to the other regions of the skin independent of hair cycle stage. Under extreme stress, however, hyperactivation of neuronal activities over-stimulates the pathway, driving MeSC depletion.

It will be interesting to determine the extent to which the mechanisms of stress-induced hair greying resemble the process of normal age-related hair greying. Similar to what we observed in stress, MeSCs also exhibit ectopic differentiation and decline in numbers in aged skins[30,59,81]. In this sense, stress might in part mimic an accelerated aging process. Of relevance, several case reports have indicated that patients who have undergone partial sympathectomy experience significantly less age-related greying on the sympathectomized side[82,83]. These case reports together with our cultured human melanocyte data suggest that sympathetic nerves and norepinephrine likely have similar impacts on MeSCs in humans. In conclusion, our findings illustrate the principles and mechanisms by which stress drives profound and permanent changes in somatic stem cells. The operative mechanisms we observed in MeSCs are likely available in

many tissues. In the future, it will be important to investigate and compare how tissue regeneration, repair, and disease progression might be altered under stress in diverse organs and tissues.

Fig. 1

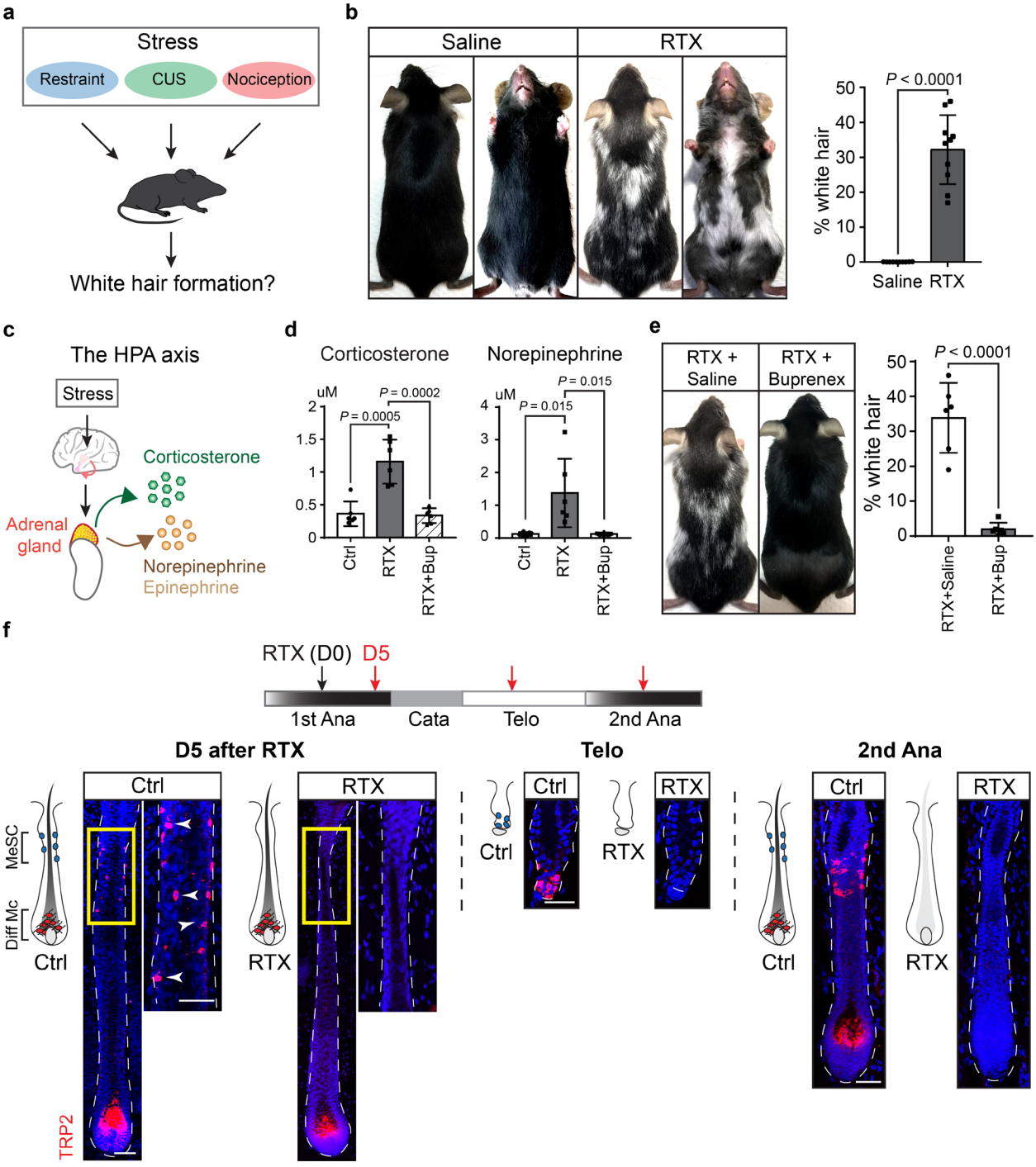

Fig. 1 | Stress induces hair greying through depletion of melanocyte stem cells (MeSCs).

a, Black coat C57/BL6 mice are subjected to different stress models to study white hair formation.

b, Hair greying after resiniferatoxin (RTX) injection. Right, quantification of the body area covered

by white hairs (n ≥ 10 mice for each condition). **c,** Schematic of the hypothalamic–pituitary–adrenal (HPA) axis. **d,** Liquid chromatography with tandem mass spectrometry (LC-MS-MS) quantifies stress hormone levels after injection of RTX alone or in combination with the analgesic buprenorphine (Buprenex) (n = 6 mice for each condition). **e,** Injection of RTX together with buprenorphine blocks grey hair formation (n ≥ 6 mice for each condition). **f,** Upper panel, schematic of experimental design (black arrow indicates RTX injection time, red arrows indicate harvesting). Lower panels, immunofluorescent staining for TRP2 (melanocyte lineage marker) in hair follicles (HFs) of control (Ctrl, Saline-injected) and RTX injected mice (≥ 30 HFs from 4-6 mice for each condition). Yellow boxes denote the bulge region where MeSCs reside. Enlarged view of the yellow box regions are shown at the right. Arrowheads indicate MeSCs. CUS: Chronic Unpredictable Stress. D: day. Bup: buprenorphine. Diff Mc: differentiated melanocytes. Scale bars, 50 μm.

Fig. 2

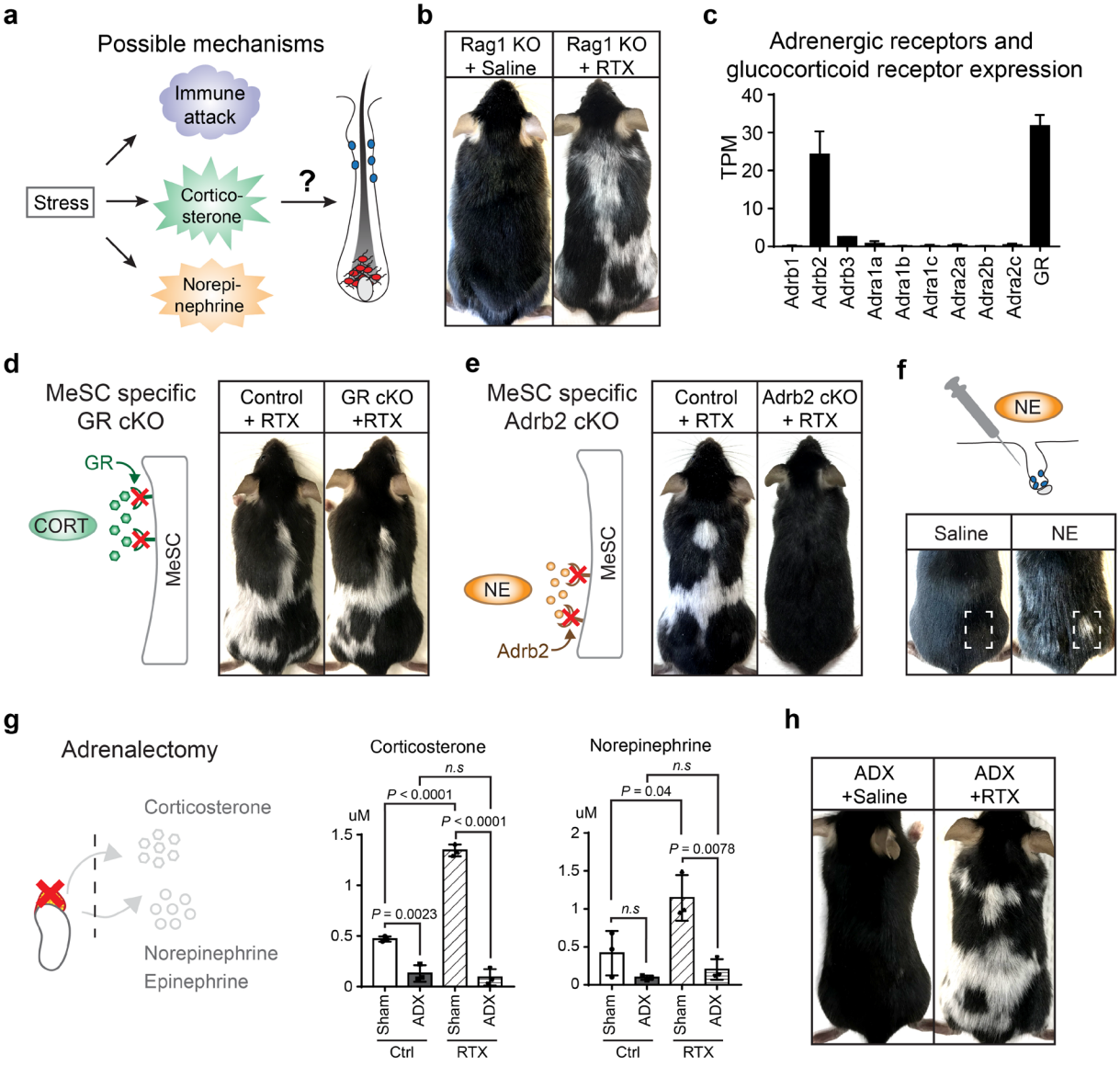

Fig. 2 | Stress-induced hair greying is mediated through norepinephrine, not corticosterone or lymphocytes-mediated immune attack. a, Schematic of possible factors influencing MeSC loss. **b,** Grey hair formation after RTX injection in Rag1 knockout mice devoid of T and B cells (Rag1 KO, n = 6 for each condition). **c,** Expression of adrenergic receptors and glucocorticoid receptor (GR) in MeSCs. **d,** White hair formation following RTX injection into Tyr-CreER; *GR* fl/fl mice (GR cKO; n = 6 for each condition). **e,** Injection of RTX into Tyr-CreER; *Adrb2* fl/fl (Adrb2 cKO) mice fails to trigger hair greying (n = 6 for each condition). **f,** White hairs

are formed after intradermal injection of norepinephrine (NE; n = 6 for each condition). White dashed boxes denote intradermal injection areas. **g,** LC-MS-MS quantification of stress hormones in sham-operated and adrenalectomized mice (n = 4 for each condition). **h,** White hair formation after RTX injection in adrenalectomized mice (ADX, n = 6 for each condition). CORT: corticosterone. NE: norepinephrine.

Fig. 3

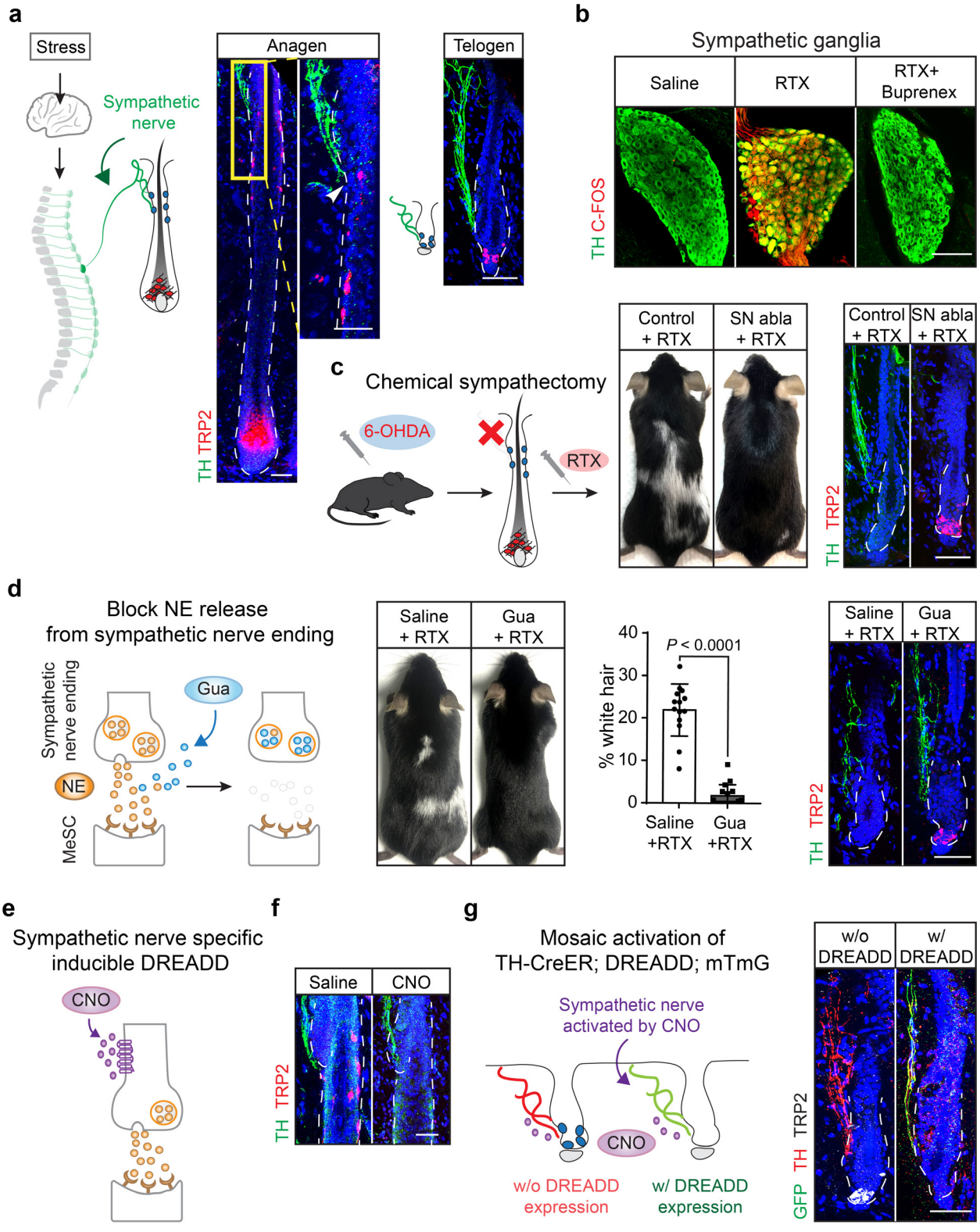
a
Stress
Sympathetic nerve
Anagen
Telogen
TH TRP2
b
Sympathetic ganglia
Saline
RTX
RTX+ Buprenex
TH C-FOS
c
Chemical sympathectomy
6-OHDA
RTX
Control + RTX
SN abla + RTX
TH TRP2
d
Block NE release from sympathetic nerve ending
Sympathetic nerve ending
Gua
NE
MeSC
Saline + RTX
Gua + RTX
P < 0.0001
% white hair
Saline +RTX
Gua +RTX
e
Sympathetic nerve specific inducible DREADD
CNO
f
Saline
CNO
TH TRP2
g
Mosaic activation of TH-CreER; DREADD; mTmG
Sympathetic nerve activated by CNO
w/o DREADD expression
w/ DREADD expression
w/o DREADD
w/ DREADD
GFP TH TRP2

Fig. 3 | Hyperactivation of sympathetic nervous system drives melanocyte stem cell depletion. a, Innervation of the MeSC niche by sympathetic nerves. Arrowhead indicates the close proximity of nerve endings to MeSCs. **b,** Immunofluorescent staining of sympathetic ganglia for tyrosine hydroxylase (TH, green) and C-FOS (red) from mice injected with vehicle, RTX, and RTX together with buprenorphine (≥ 30 sympathetic ganglia total from 4-6 mice for each condition). **c,** 6-hydroxydopamine (6-OHDA) injection blocks grey hair induction by RTX (n = 6 mice for each condition; immunofluorescent analyses: ≥ 30 HFs from 4-6 mice for each condition). d, Guanethidine (Gua) injection blocks formation of grey hair induced by RTX injection (n = 14 mice for each condition; immunofluorescent analyses: ≥ 30 HFs from 4-6 mice for each condition) **e,** Schematic of DREADD system. **f,** Immunofluorescent staining of HFs for TH (green) and TRP2 (red) from TH-CreER; DREADD mice treated with saline or Clozapine N-Oxide (CNO, ≥ 30 HFs from 4 - 6 mice). **g,** Mosaic activation of sympathetic nerve using TH-CreER; DREADD; mTmG mice. Note that MeSCs disappear only from hair follicles innervated with sympathetic nerves expressing DREADD (marked by membrane GFP expression, ≥ 30 HFs from 4 - 6 mice). SN abla: sympathetic nerve ablation. Scale bars, 50 μm.

Fig. 4

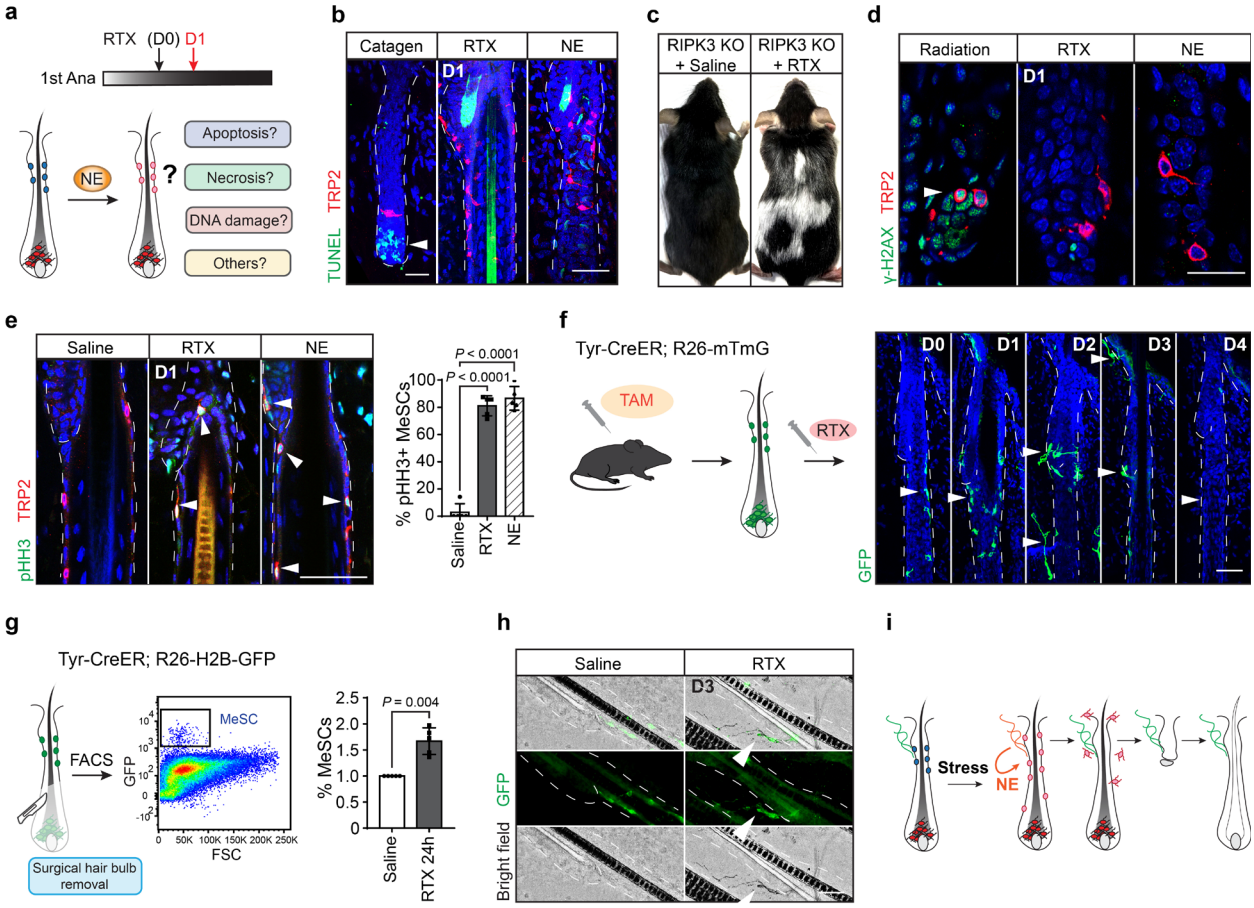

Fig. 4 | Norepinephrine drives MeSCs out of their quiescent state. a, Schematic of possible mechanisms that lead to MeSC loss by norepinephrine (NE). **b,** Terminal deoxynucleotidyl transferase dUTP nick end labelling (TUNEL) assay of HFs from mice 1 day after RTX or NE treatment. Catagen HFs are used as positive controls for TUNEL. White arrowhead points to apoptotic hair follicle cells. **c,** White hair formation in RIPK3 knockout mice (RIPK3 KO) injected with RTX (n = 5). **d,** Immunofluorescent staining of HFs for the DNA damage marker γ-H2AX (green) and TRP2 (red) from mice 1 day after RTX or NE treatment. HFs from irradiated mice are used as positive controls. White arrowhead indicates the MeSCs with DNA damage. **e,** Immunofluorescent staining of HFs for phospho-Histone H3 (pHH3, green) and TRP2 (red) from mice 1 day after RTX or NE injection. White arrowhead highlights the proliferative MeSCs. **f,** Lineage tracing time course of MeSCs after RTX treatment using Tyr-CreER; mTmG. White

arrowheads mark MeSCs after RTX treatment. **g,** Left, schematic of MeSCs isolation strategy. Right panel, FACS quantification of MeSCs 24 hrs after RTX (n = 5 for each condition). **h,** Immunofluorescent and brightfield images of HFs from mice 3 days after RTX injection. White arrowheads indicate ectopically differentiated MeSCs with pigmentation. **I,** Model for NE-mediated MeSC loss from hair follicle. TAM: tamoxifen. Scale bars, 50 μm.

Fig. 5

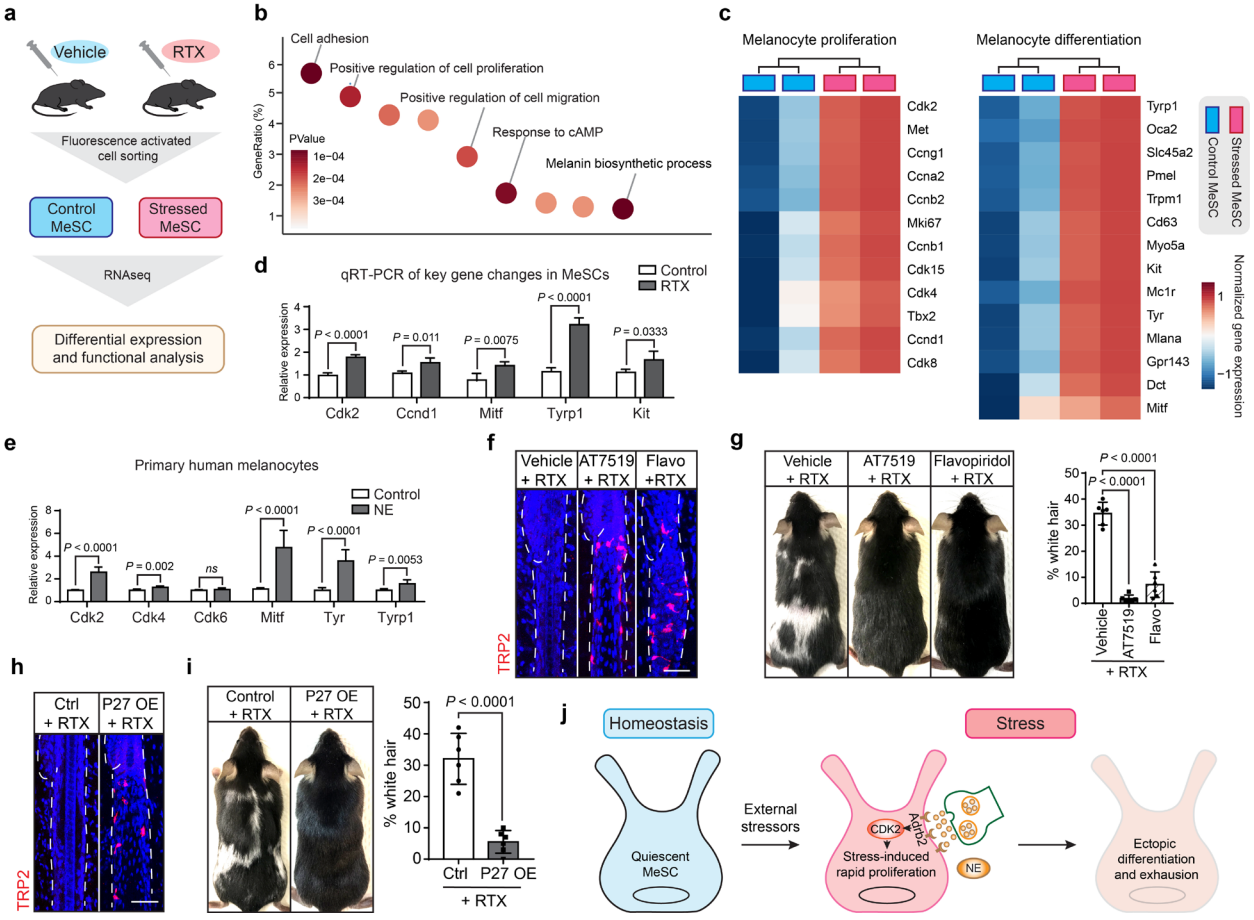

Fig. 5 | MeSCs up-regulate proliferation and differentiation programs upon RTX injection. **a,** Schematic of experimental workflow for FASC-isolation of MeSCs and RNAseq. **b,** Gene ontology (GO) analysis of significantly deregulated genes in stressed MeSCs. **c,** Heatmaps illustrating expression of signature genes related to MeSC proliferation and differentiation. **d,** qRT-PCR validation of selected differentially expressed genes in FACS-purified mouse MeSCs. **e,** qRT-PCR of MeSC-related proliferation and differentiation genes in cultured primary human melanocytes treated with norepinephrine (NE). **f,** Immunofluorescent staining of HFs for TRP2 (red) from mice 5-7 days after treatment of RTX together with AT7519 or Flavopiridol (≥ 30 HFs from 6 mice). **g,** Topical treatment of AT7519 or Flavopiridol inhibits RTX-induced hair greying (n=6 for each condition). **h,** Immunofluorescent staining of HFs for TRP2 (red) from P27 OE 5 days after treatment of RTX (≥ 30 HFs from 6 mice). **I,** P27 overexpression (P27 OE) together

with RTX injection blocks hair greying (n=6 for each condition). **j,** Model summarizing the main findings. Under the influence of strong external stressors, activated sympathetic nerves secrete norepinephrine that binds to Adrb2 on MeSCs. NE-Adrb2 signalling drive rapid MeSC proliferation, which leads to their ectopic differentiation and exhaustion. Scale bars, 50 μm.

METHODS

Animals

C57BL/6, Tyr-CreER[36], K15-CrePGR[84], Rag1 KO[85], CD11b-DTR[86], GR flox[87], Dreadd flox[49], Rosa-H2BGFP/mCherry[88], Rosa-mTmG[89], Rosa-rtTA, and RIPK3 knockout mice were obtained from the Jackson Laboratory. Adrb2 flox[90] mice were originally generated by Gerard Karsenty (Columbia University) and provided to us by Paul Frenette (Albert Einstein College of Medicine). TH-CreER[91] mice were generated and provided by David Ginty (Harvard Medical School). TetO-P27 mice were originally generated and donated to the Jackson laboratory by Gillian K. Cady (Roswell Park Cancer Institute)[92], and provided to us by Valentina Greco (Yale School of Medicine). All experiments used balanced groups of male and female mice. All animals were maintained in an Association for Assessment and Accreditation of Laboratory Animal Care-approved animal facility at Harvard University, Harvard medical school, and ethical committee from Ribeirao Preto Medical School (Protocol n. 046/2019). Procedures were approved by Institutional Animal Care and Use Committee of all institutions.

Stress procedures

Restraint and Chronic Unpredictable Stress (CUS) procedure were performed as previously described[12–15]. Briefly, for restraint stress, C57BL/6 mice were kept in a mouse restrainer (Fisher Scientific 12972590) for 4 hours a day for a week starting from mid-anagen. Mice were waxed to induce hair regeneration when their hair cycle reached telogen. Mice were waxed 4 times in total. For CUS, C57BL/6 mice were exposed to a combination of stressors according to the CUS timetable. Two of the stressors are applied each day. The stressors include cage tilt, isolation, crowding, damp bedding, rapid light/dark changes, overnight illumination, restraining, empty cage and 3x cage change. All stressors were randomly repeated in consecutive weeks. Nociception induction by RTX was performed as previous described[20,93,94]: mice received injections of resiniferatoxin (30-100 μg/kg) in the flank for 1-3 days. RTX was prepared in 2% DMSO with 0.15% Tween 80 in PBS. Control mice were treated with vehicle only.

Histology and immunohistochemistry

Mouse skin samples were fixed using 4% paraformaldehyde (PFA) for 15 minutes at room temperature, washed 6 times with PBS and immersed in 30% sucrose overnight at 4°C. Samples were then embedded in OCT (Sakura Finetek). 35 µM section were fixed in 4% paraformaldehyde (PFA) for 2 minutes and washed with PBS and PBST. Slides were then blocked using blocking buffer (5% Donkey serum; 1% BSA, 2% Cold water fish gelatin in 0.3% Triton in PBS) for 1 hour at room temperature, incubated with primary antibodies overnight at 4°C and secondary antibody for 4 hours at room temperature. EdU was developed for 1 hour, using Click-It reaction according to manufacturer instructions (Thermo Fisher Scientific). TUNEL assay was performed according to manufacture instruction (Roche 11684795910). Antibodies used: TRP2 (Santa Cruz 10451, 1:400), Tyrosine hydroxylase (rabbit, Millipore AB152, 1:1000 or sheep, Millipore AB1542, 1:150-1:300), c-fos (Abcam, 190289), γ-H2AX (Cell Signaling, 9718), phospho-histone H3 (rabbit, Cell Signaling Technology 3377S, 1:250), cleaved Caspase 3 (rabbit, Cell Signaling Technology 9664S, 1:100-1:300), GFP (rabbit, Abcam ab290, 1:5000 or chicken, Aves labs GFP-1010, 1:200), CD3 (eBioscience 14-0032-81, 1:400), CD11b (eBioscience 14-0112-81, 1:400).

Measurement of stress hormones

50 µl of blood plasma was collected and transferred into a 1.5 ml microcentrifuge tube. 10 µl of internals solution is added to each sample followed by 100 µl of water and 640 µl of methanol. Samples are incubated at -20°C for 1 hour, then centrifuged 30 minutes at maximum speed at -9°C. The supernatant is transferred to a new tube and dried under N2 flow and resuspended in 50 µl methanol and transferred to micro-inserts. All samples were run on an Agilent 6460 Triple Quad LC/MS with an Agilent 1290 Infinity HPLC.

Analgesia

Mice were injected with buprenorphine (0.2 mg/kg) 4 hours before RTX injection, and every 6 hours after RTX injection for 2 days.

Tamoxifen treatment

Tamoxifen was diluted in corn oil to a final concentration of 20 mg/ml. To induce recombination, 20 mg/kg was injected intraperitoneally once per day for 4-6 days.

Intradermal norepinephrine injection

Norepinephrine (Sigma-Aldrich 489350) solution was prepared freshly by dissolving in 0.1% ascorbic acid in 0.9% sterile NaCl to a final concentration of 2 mM. 50 µl was injected intradermally into experimental animals together with fluorescent beads. Control animals were injected with equivalent volume of vehicle (0.1% ascorbic acid in 0.9% sterile NaCl).

Sympathetic nerve ablation

6-Hydroxydopamine hydrobromide (6-OHDA, Sigma 162957) solution was prepared freshly by dissolving 6-OHDA in 0.1% ascorbic acid in 0.9% sterile NaCl. 100 mg/kg (body weight) of 6-OHDA were injected intraperitoneally daily from P18 to P22. Control animals were injected with equivalent volume of vehicle (0.1% ascorbic acid in 0.9% sterile NaCl).

Guanethidine treatment

Mice were intraperitoneally injected with 30 mg/kg (body weight) of guanethidine (Sigma-Aldrich, 1301801), once a day for 3 consecutive days prior to RTX administration.

Induction of Dreadd

CNO (20 mg/kg body weight) was injected intraperitoneally daily from P21-P30. Control animals were injected with equivalent volume of vehicle (0.9% sterile NaCl).

Diphtheria toxin administration

Diphtheria toxin (Sigma-Aldrich) was dissolved in 0.9% NaCl (0.1 mg/ml). For ablation, CD11b-DTR transgenic mice were intraperitoneally injected with 25 ng/g (body weight) diphtheria toxin daily 3 days before RTX injection and continued every three days for a total of 6 times.

Radiation

Ten weeks old C56Bl/6J mice were gamma irradiated (137-Cs source) with a split 10.5 gray split dose. Mice were transplanted with 300,000 whole bone marrow cells to ensure survival after lethal irradiation.

Inhibitor treatment

To ensure inhibition of MeSC proliferation, mice were shaved and pre-treated with 5 mg/kg (body weight) AT7519 (Cayman Chemical 16231) or Flavopiridol (Cayman Chemical 10009197) in ethanol topically 48 hours and 24 hours before RTX injection, at the time of RTX injection, and 24 hours and 48 hours after injection.

FACS

Mouse dorsal skin was collected, and the fat layer was removed by gentle scrapping from dermal side. The skin was incubated in trypsin-EDTA at 37 °C for 35-45 minutes on an orbital shaker. Single cell suspension was collected by gentle scrapping of the dermal side and filter through 70 μm and 40 μm filters. Single cell suspension was centrifuged for 5 minutes at 4°C, resuspended in 0.25% FBS in PBS and stained with fluorescent dye-conjugated antibodies for 30 minutes.

RNA isolation

RNA was isolated using RNeasy micro Kit (Qiagen), using QIAcube according to manufacturer instruction. RNA concentration and RNA integrity were determined by Bioanalyzer (Agilent, Santa Clara, CA) using the RNA 6000 Nano chip. High quality RNA samples with RNA Integrity Number ≥ 8 were used as input for RT-PCR and RNA-sequencing.

Cell Culture

Primary human melanocytes between passages 2 and 4 were derived from neonatal and cultured in Medium 254 (Invitrogen, Thermo Fisher Scientific) to maintain in an undifferentiated state. The cells were starved for 24 hours in HAM's F-10 + 1% penicillin/streptomycin/glutamine before adding NE (10uM). All experiments involving human samples were approved by Institutional Review Board of Massachusetts General Hospital.

Quantitative real-time PCR

The cDNA libraries were synthesized using Superscript IV VILO master mix with ezDNase (Thermo Fisher). Quantitative real time PCR was performed using power SYBR green (Thermo Fisher). Ct values were normalized to beta-actin.

Imaging and image analysis

All images were acquired using Zeiss LSM 880 confocal microscope or Keyence microscope using x20 or x40 magnification lenses. Images are presented as Maximum Intensity Projection image or a single Z stack.

Statistical analysis

Statistical analyses were performed with Prism using unpaired two-tailed Student's t-test. The data are presented as mean ± SD.

RNA-seq computational analysis

The reads were trimmed using Trim Galore! (https://www.bioinformatics.babraham.ac.uk/projects/trim_galore/) and aligned to the mouse reference genome (mm10) with STAR aligner[95]. Reads with alignment quality < Q30 are discarded. The gene expression levels are normalized, and differential genes are calculated using DEseq2[96]. Gene set functional enrichment analysis was performed using David[97,98].

Data Availability

RNA-seq datasets have been deposited online in the Gene Expression Omnibus (GEO) under accession numbers X.

References

1. Ephraim, A. J. On Sudden or Rapid Whitening of the Hair. *AMA Arch Derm* **79**, 228–236 (1959).
2. Takeo, M. *et al.* EdnrB Governs Regenerative Response of Melanocyte Stem Cells by Crosstalk with Wnt Signaling. *Cell Reports* **15**, 1291–1302 (2016).
3. Moon, H. *et al.* Melanocyte Stem Cell Activation and Translocation Initiate Cutaneous Melanoma in Response to UV Exposure. *Cell Stem Cell* **21**, 665-678.e6 (2017).
4. Köhler, C. *et al.* Mouse Cutaneous Melanoma Induced by Mutant BRaf Arises from Expansion and Dedifferentiation of Mature Pigmented Melanocytes. *Cell Stem Cell* **21**, 679-693.e6 (2017).
5. Dankort, D. *et al.* BRafV600E cooperates with Pten silencing to elicit metastatic melanoma. *Nature genetics* **41**, 544 (2009).
6. Nishimura, E. K. *et al.* Dominant role of the niche in melanocyte stem-cell fate determination. *Nature* **416**, 854 (2002).
7. Zocco, M. & Blanpain, C. Identifying the niche controlling melanocyte differentiation. *Genes Dev.* **31**, 721–723 (2017).
8. Chang, C.-Y. *et al.* NFIB is a governor of epithelial–melanocyte stem cell behaviour in a shared niche. *Nature* **495**, 98–102 (2013).
9. Rabbani, P. *et al.* Coordinated Activation of Wnt in Epithelial and Melanocyte Stem Cells Initiates Pigmented Hair Regeneration. *Cell* **145**, 941–955 (2011).
10. Hsu, Y.-C., Li, L. & Fuchs, E. Emerging interactions between skin stem cells and their niches. *Nature Medicine* **20**, 847–856 (2014).

11. Qiu, W., Chuong, C.-M. & Lei, M. Regulation of melanocyte stem cells in the pigmentation of skin and its appendages: Biological patterning and therapeutic potentials. *Experimental Dermatology* **28**, 395–405 (2019).
12. Anthony, T. E. *et al.* Control of Stress-Induced Persistent Anxiety by an Extra-Amygdala Septohypothalamic Circuit. *Cell* **156**, 522–536 (2014).
13. Ramirez, S. *et al.* Activating positive memory engrams suppresses depression-like behaviour. *Nature* **522**, 335–339 (2015).
14. Heidt, T. *et al.* Chronic variable stress activates hematopoietic stem cells. *Nat Med* **20**, 754–758 (2014).
15. Tye, K. M. *et al.* Dopamine neurons modulate neural encoding and expression of depression-related behaviour. *Nature* **493**, 537–541 (2013).
16. Bondi, C. O., Rodriguez, G., Gould, G. G., Frazer, A. & Morilak, D. A. Chronic Unpredictable Stress Induces a Cognitive Deficit and Anxiety-Like Behavior in Rats that is Prevented by Chronic Antidepressant Drug Treatment. *Neuropsychopharmacology* **33**, 320–331 (2008).
17. Hollon, N. G., Burgeno, L. M. & Phillips, P. E. M. Stress effects on the neural substrates of motivated behavior. *Nat Neurosci* **18**, 1405–1412 (2015).
18. Szallasi, A. & Blumberg, P. M. Resiniferatoxin, a phorbol-related diterpene, acts as an ultrapotent analog of capsaicin, the irritant constituent in red pepper. *Neuroscience* **30**, 515–520 (1989).
19. Acs, G., Biro, T., Acs, P., Modarres, S. & Blumberg, P. M. Differential Activation and Desensitization of Sensory Neurons by Resiniferatoxin. *J. Neurosci.* **17**, 5622–5628 (1997).

20. Baral, P. *et al.* Nociceptor sensory neurons suppress neutrophil and γδ T cell responses in bacterial lung infections and lethal pneumonia. *Nature Medicine* (2018). doi:10.1038/nm.4501
21. Ulrich-Lai, Y. M. & Herman, J. P. Neural regulation of endocrine and autonomic stress responses. *Nature Reviews Neuroscience* **10**, 397–409 (2009).
22. Hermes, G. L. *et al.* Social isolation dysregulates endocrine and behavioral stress while increasing malignant burden of spontaneous mammary tumors. *PNAS* **106**, 22393–22398 (2009).
23. Volden, P. A. & Conzen, S. D. The influence of glucocorticoid signaling on tumor progression. *Brain, Behavior, and Immunity* **30**, S26–S31 (2013).
24. Marshall, I. C. B. *et al.* Activation of vanilloid receptor 1 by resiniferatoxin mobilizes calcium from inositol 1,4,5-trisphosphate-sensitive stores. *British Journal of Pharmacology* **138**, 172–176 (2003).
25. Neubert, J. *et al.* Peripherally induced resiniferatoxin analgesia. *Pain* **104**, 219–228 (2003).
26. WATANABE, T., SAKURADA, N. & KOBATA, K. Capsaicin-, Resiniferatoxin-, and Olvanil-induced Adrenaline Secretions in Rats via the Vanilloid Receptor. *Bioscience, Biotechnology, and Biochemistry* **65**, 2443–2447 (2001).
27. Hearing, V. J. Biogenesis of pigment granules: a sensitive way to regulate melanocyte function. *Journal of Dermatological Science* **37**, 3–14 (2005).
28. Hirobe, T. How are proliferation and differentiation of melanocytes regulated? *Pigment Cell & Melanoma Research* **24**, 462–478 (2011).
29. Kondo, T. & Hearing, V. J. Update on the regulation of mammalian melanocyte function and skin pigmentation. *Expert Rev Dermatol* **6**, 97–108 (2011).

30. Steingrímsson, E., Copeland, N. G. & Jenkins, N. A. Melanocyte Stem Cell Maintenance and Hair Graying. *Cell* **121**, 9–12 (2005).
31. Liao, C.-P., Booker, R. C., Morrison, S. J. & Le, L. Q. Identification of hair shaft progenitors that create a niche for hair pigmentation. *Genes Dev.* **31**, 744–756 (2017).
32. Inomata, K. *et al.* Genotoxic Stress Abrogates Renewal of Melanocyte Stem Cells by Triggering Their Differentiation. *Cell* **137**, 1088–1099 (2009).
33. Harris, M. L. *et al.* A direct link between MITF, innate immunity, and hair graying. *PLOS Biology* **16**, e2003648 (2018).
34. Navarini, A. A. & Nobbe, S. Marie Antoinette Syndrome. *Arch Dermatol* **145**, 656–656 (2009).
35. Glaser, R. & Kiecolt-Glaser, J. K. Stress-induced immune dysfunction: implications for health. *Nature Reviews Immunology* **5**, 243 (2005).
36. Bosenberg, M. *et al.* Characterization of melanocyte-specific inducible Cre recombinase transgenic mice. *genesis* **44**, 262–267 (2006).
37. Ceasrine, A. M., Lin, E. E., Lumelsky, D. N., Iyer, R. & Kuruvilla, R. Adrb2 controls glucose homeostasis by developmental regulation of pancreatic islet vasculature. *eLife* **7**, e39689 (2018).
38. Katayama, Y. *et al.* Signals from the Sympathetic Nervous System Regulate Hematopoietic Stem Cell Egress from Bone Marrow. *Cell* **124**, 407–421 (2006).
39. Maryanovich, M. *et al.* Adrenergic nerve degeneration in bone marrow drives aging of the hematopoietic stem cell niche. *Nature Medicine* **24**, 782 (2018).
40. Zeng, X. *et al.* Innervation of thermogenic adipose tissue via a calsyntenin 3β–S100b axis. *Nature* **569**, 229 (2019).

41. Zweifel, L. S., Kuruvilla, R. & Ginty, D. D. Functions and mechanisms of retrograde neurotrophin signalling. *Nature Reviews Neuroscience* **6**, 615 (2005).
42. Sheng, M. & Greenberg, M. E. The regulation and function of c-fos and other immediate early genes in the nervous system. *Neuron* **4**, 477–485 (1990).
43. Sheng, M., McFadden, G. & Greenberg, M. E. Membrane depolarization and calcium induce c-fos transcription via phosphorylation of transcription factor CREB. *Neuron* **4**, 571–582 (1990).
44. Kostrzewa, R. M. & Jacobowitz, D. M. Pharmacological Actions of 6-Hydroxydopamine. *Pharmacol Rev* **26**, 199–288 (1974).
45. Boullin, D. J., Costa, E. & Brodie, B. B. Discharge of tritium-labeled guanethidine by sympathetic nerve stimulation as evidence that guanethidine is a false transmitter. *Life Sciences* **5**, 803–808 (1966).
46. Johnson, E. M., Cantor, E. & Douglas, J. R. Biochemical and functional evaluation of the sympathectomy produced by the administration of guanethidine to newborn rats. *J Pharmacol Exp Ther* **193**, 503–512 (1975).
47. Maxwell, R. A., Plummer, A. J., Schneider, F., Povalski, H. & Daniel, A. I. Pharmacology of [2-(octahydro-1-Azocinvl)-Ethyl-Guanidine Sulfate (su-5864). *J Pharmacol Exp Ther* **128**, 22–29 (1960).
48. Roth, B. L. DREADDs for Neuroscientists. *Neuron* **89**, 683–694 (2016).
49. Zhu, H. *et al.* Cre-dependent DREADD (Designer Receptors Exclusively Activated by Designer Drugs) mice. *genesis* **54**, 439–446 (2016).
50. Acar, M. *et al.* Deep imaging of bone marrow shows non-dividing stem cells are mainly perisinusoidal. *Nature* **526**, 126–130 (2015).

51. Baldridge, M. T., King, K. Y., Boles, N. C., Weksberg, D. C. & Goodell, M. A. Quiescent hematopoietic stem cells are activated by IFNγ in response to chronic infection. *Nature* **465**, 793–797 (2010).

52. Cheung, T. H. & Rando, T. A. Molecular regulation of stem cell quiescence. *Nature Reviews Molecular Cell Biology* **14**, 329–340 (2013).

53. Lay, K., Kume, T. & Fuchs, E. FOXC1 maintains the hair follicle stem cell niche and governs stem cell quiescence to preserve long-term tissue-regenerating potential. *PNAS* **113**, E1506–E1515 (2016).

54. Wang, L., Siegenthaler, J. A., Dowell, R. D. & Yi, R. Foxc1 reinforces quiescence in self-renewing hair follicle stem cells. *Science* **351**, 613–617 (2016).

55. Lowry, W. E., Flores, A. & White, A. C. Exploiting Mouse Models to Study Ras-Induced Cutaneous Squamous Cell Carcinoma. *J Invest Dermatol* **136**, 1543–1548 (2016).

56. White, A. C. *et al.* Stem cell quiescence acts as a tumour suppressor in squamous tumours. *Nature Cell Biology* **16**, 99–107 (2014).

57. Bernitz, J. M., Kim, H. S., MacArthur, B., Sieburg, H. & Moore, K. Hematopoietic Stem Cells Count and Remember Self-Renewal Divisions. *Cell* **167**, 1296-1309.e10 (2016).

58. Chakkalakal, J. V., Jones, K. M., Basson, M. A. & Brack, A. S. The aged niche disrupts muscle stem cell quiescence. *Nature* **490**, 355–360 (2012).

59. Nishimura, E. K., Granter, S. R. & Fisher, D. E. Mechanisms of Hair Graying: Incomplete Melanocyte Stem Cell Maintenance in the Niche. *Science* **307**, 720–724 (2005).

60. Nishimura, E. K. *et al.* Key Roles for Transforming Growth Factor β in Melanocyte Stem Cell Maintenance. *Cell Stem Cell* **6**, 130–140 (2010).

61. Macosko, E. Z. *et al.* Highly parallel genome-wide expression profiling of individual cells using nanoliter droplets. *Cell* **161**, 1202–1214 (2015).

62. Tirosh, I. *et al.* Dissecting the multicellular ecosystem of metastatic melanoma by single-cell RNA-seq. *Science* **352**, 189–196 (2016).

63. Whitfield, M. L., George, L. K., Grant, G. D. & Perou, C. M. Common markers of proliferation. *Nature Reviews Cancer* **6**, 99 (2006).

64. Du, J. *et al.* Critical role of CDK2 for melanoma growth linked to its melanocyte-specific transcriptional regulation by MITF. *Cancer Cell* **6**, 565–576 (2004).

65. Losiewicz, M. D., Carlson, B. A., Kaur, G., Sausville, E. A. & Worland, P. J. Potent Inhibition of Cdc2 Kinase Activity by the Flavonoid L86-8275. *Biochemical and Biophysical Research Communications* **201**, 589–595 (1994).

66. Wyatt, P. G. *et al.* Identification of N-(4-Piperidinyl)-4-(2,6-dichlorobenzoylamino)-1H-pyrazole-3-carboxamide (AT7519), a Novel Cyclin Dependent Kinase Inhibitor Using Fragment-Based X-Ray Crystallography and Structure Based Drug Design. *J. Med. Chem.* **51**, 4986–4999 (2008).

67. Brown, S. *et al.* Correction of aberrant growth preserves tissue homeostasis. *Nature* **548**, 334–337 (2017).

68. Xin, T., Gonzalez, D., Rompolas, P. & Greco, V. Flexible fate determination ensures robust differentiation in the hair follicle. *Nature Cell Biology* **20**, 1361 (2018).

69. Borden, P., Houtz, J., Leach, S. D. & Kuruvilla, R. Sympathetic innervation during development is necessary for pancreatic islet architecture and functional maturation. *Cell Rep* **4**, 287–301 (2013).

70. Maryanovich, M., Takeishi, S. & Frenette, P. S. Neural Regulation of Bone and Bone Marrow. *Cold Spring Harb Perspect Med* **8**, a031344 (2018).

71. Hanoun, M., Maryanovich, M., Arnal-Estapé, A. & Frenette, P. S. Neural Regulation of Hematopoiesis, Inflammation, and Cancer. *Neuron* **86**, 360–373 (2015).

72. Mendez-Ferrer, S., Enikolopov, G. N., Lira, S. & Frenette, P. S. Mesenchymal Stem Cells, Regulated by the Sympathetic Nervous System, Form the Hematopoietic Stem Cell Niche. *Blood* **112**, 4–4 (2008).

73. Reed, C. M. The ultrastructure and innervation of muscles controlling chromatophore expansion in the squid, Loligo vulgaris. *Cell Tissue Res.* **282**, 503–512 (1995).

74. Sanders, G. D. & Young, J. Z. Reappearance of specific colour patterns after nerve regeneration in Octopus. *Proc. R. Soc. Lond., B, Biol. Sci.* **186**, 1–11 (1974).

75. Logan, D. W., Burn, S. F. & Jackson, I. J. Regulation of pigmentation in zebrafish melanophores. *Pigment Cell Research* **19**, 206–213 (2006).

76. Singh, A. P. & Nüsslein-Volhard, C. Zebrafish Stripes as a Model for Vertebrate Colour Pattern Formation. *Current Biology* **25**, R81–R92 (2015).

77. Chou, W. C. *et al.* Direct migration of follicular melanocyte stem cells to the epidermis after wounding or UVB irradiation is dependent on Mc1r signaling. *Nature Medicine* **19**, 924–929 (2013).

78. Lo, J. A. & Fisher, D. E. The melanoma revolution: From UV carcinogenesis to a new era in therapeutics. *Science* **346**, 945–949 (2014).

79. Fan, S. M.-Y. *et al.* External light activates hair follicle stem cells through eyes via an ipRGC–SCN–sympathetic neural pathway. *PNAS* **115**, E6880–E6889 (2018).

80. Saito, Y. *et al.* Effect of bright light exposure on muscle sympathetic nerve activity in human. *Neuroscience Letters* **219**, 135–137 (1996).

81. Sarin, K. Y. & Artandi, S. E. Aging, graying and loss of melanocyte stem cells. *Stem Cell Rev* **3**, 212–217 (2007).

82. Lerner, A. B. Gray hair and sympathectomy. Report of a case. *Arch Dermatol* **93**, 235–236 (1966).

83. Ortonne, J. P., Thivolet, J. & Guillet, R. Graying of hair with age and sympathectomy. *Arch Dermatol* **118**, 876–877 (1982).

84. Morris, R. J. *et al.* Capturing and profiling adult hair follicle stem cells. *Nature Biotechnology* **22**, 411 (2004).

85. Mombaerts, P. *et al.* RAG-1-deficient mice have no mature B and T lymphocytes. *Cell* **68**, 869–877 (1992).

86. Duffield, J. S. *et al.* Selective depletion of macrophages reveals distinct, opposing roles during liver injury and repair. *J Clin Invest* **115**, 56–65 (2005).

87. Mittelstadt, P. R., Monteiro, J. P. & Ashwell, J. D. Thymocyte responsiveness to endogenous glucocorticoids is required for immunological fitness. *J Clin Invest* **122**, 2384–2394 (2012).

88. Chen, Y.-T. *et al.* R26R-GR: A Cre-Activable Dual Fluorescent Protein Reporter Mouse. *PLOS ONE* **7**, e46171 (2012).

89. Muzumdar, M. D., Tasic, B., Miyamichi, K., Li, L. & Luo, L. A global double-fluorescent Cre reporter mouse. *genesis* **45**, 593–605 (2007).

90. Hinoi, E. *et al.* The sympathetic tone mediates leptin's inhibition of insulin secretion by modulating osteocalcin bioactivity. *J Cell Biol* **183**, 1235–1242 (2008).

91. Abraira, V. E. *et al.* The Cellular and Synaptic Architecture of the Mechanosensory Dorsal Horn. *Cell* **168**, 295-310.e19 (2017).

92. Pruitt, S. C., Freeland, A., Rusiniak, M. E., Kunnev, D. & Cady, G. K. Cdkn1b overexpression in adult mice alters the balance between genome and tissue ageing. *Nat Commun* **4**, 2626 (2013).

93. Riol-Blanco, L. *et al.* Nociceptive sensory neurons drive interleukin-23-mediated psoriasiform skin inflammation. *Nature* **510**, 157–161 (2014).

94. Kashem, S. W. *et al.* Nociceptive Sensory Fibers Drive Interleukin-23 Production from CD301b+ Dermal Dendritic Cells and Drive Protective Cutaneous Immunity. *Immunity* **43**, 515–526 (2015).

95. Dobin, A. *et al.* STAR: ultrafast universal RNA-seq aligner. *Bioinformatics* **29**, 15–21 (2013).

96. Love, M. I., Huber, W. & Anders, S. Moderated estimation of fold change and dispersion for RNA-seq data with DESeq2. *Genome Biology* **15**, 550 (2014).

97. Huang, D. W., Sherman, B. T. & Lempicki, R. A. Bioinformatics enrichment tools: paths toward the comprehensive functional analysis of large gene lists. *Nucleic Acids Res.* **37**, 1–13 (2009).

98. Huang, D. W., Sherman, B. T. & Lempicki, R. A. Systematic and integrative analysis of large gene lists using DAVID bioinformatics resources. *Nat Protoc* **4**, 44–57 (2009).

Extended Data Fig. 1

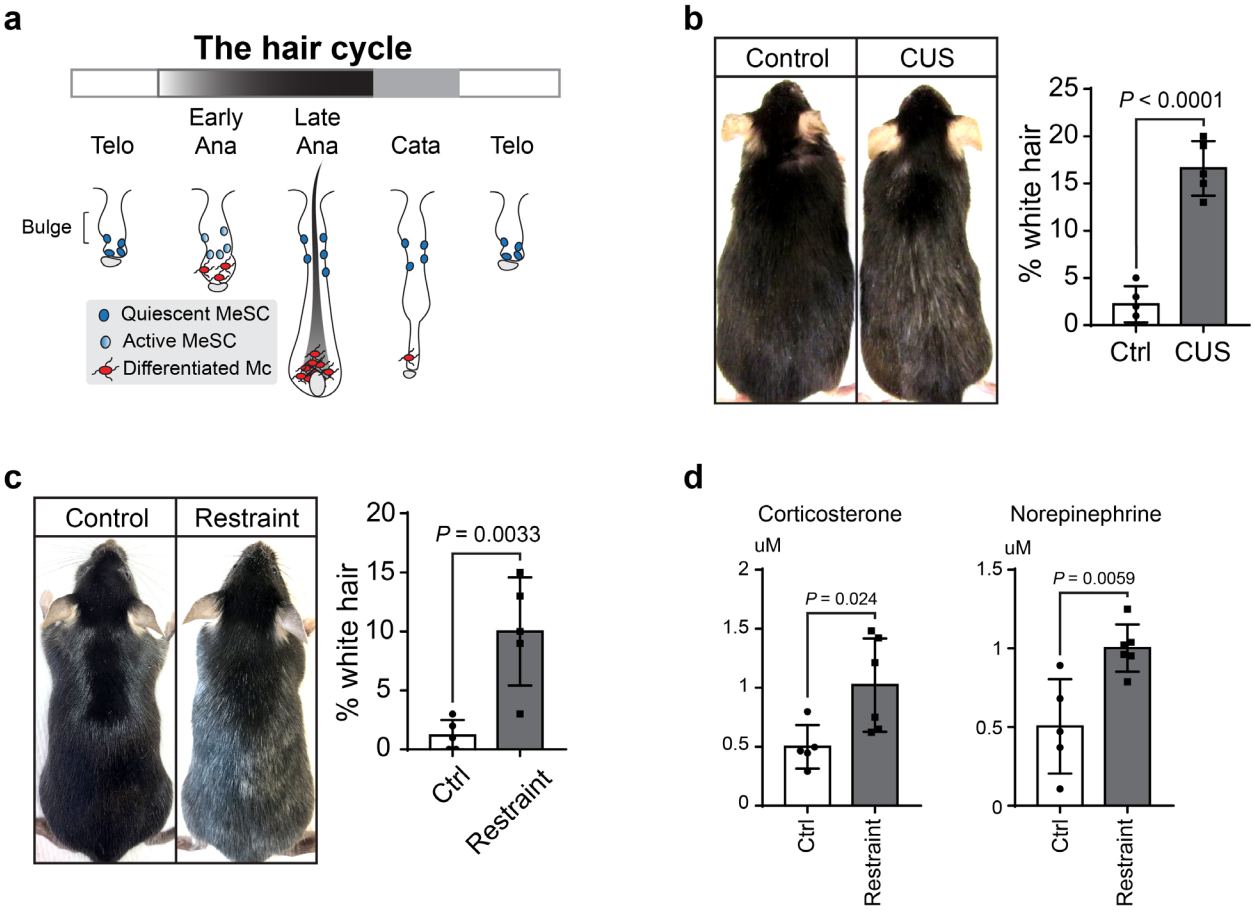

Extended Data Fig. 1 | The hair cycle, induction of hair greying by chronic unpredictable stress (CUS) and restraint and quantification of stress hormones. a, Schematic of MeSCs behaviour during hair cycle. **b,** Hair greying after mice are subjected to CUS (n = 5 for each condition). **c,** Hair greying after mice are subjected to restraint stress (n = 5 for each condition). **d,** LC-MS-MS quantification of corticosterone and norepinephrine after restraint stress (n = 6 for each condition).

Extended Data Fig. 2

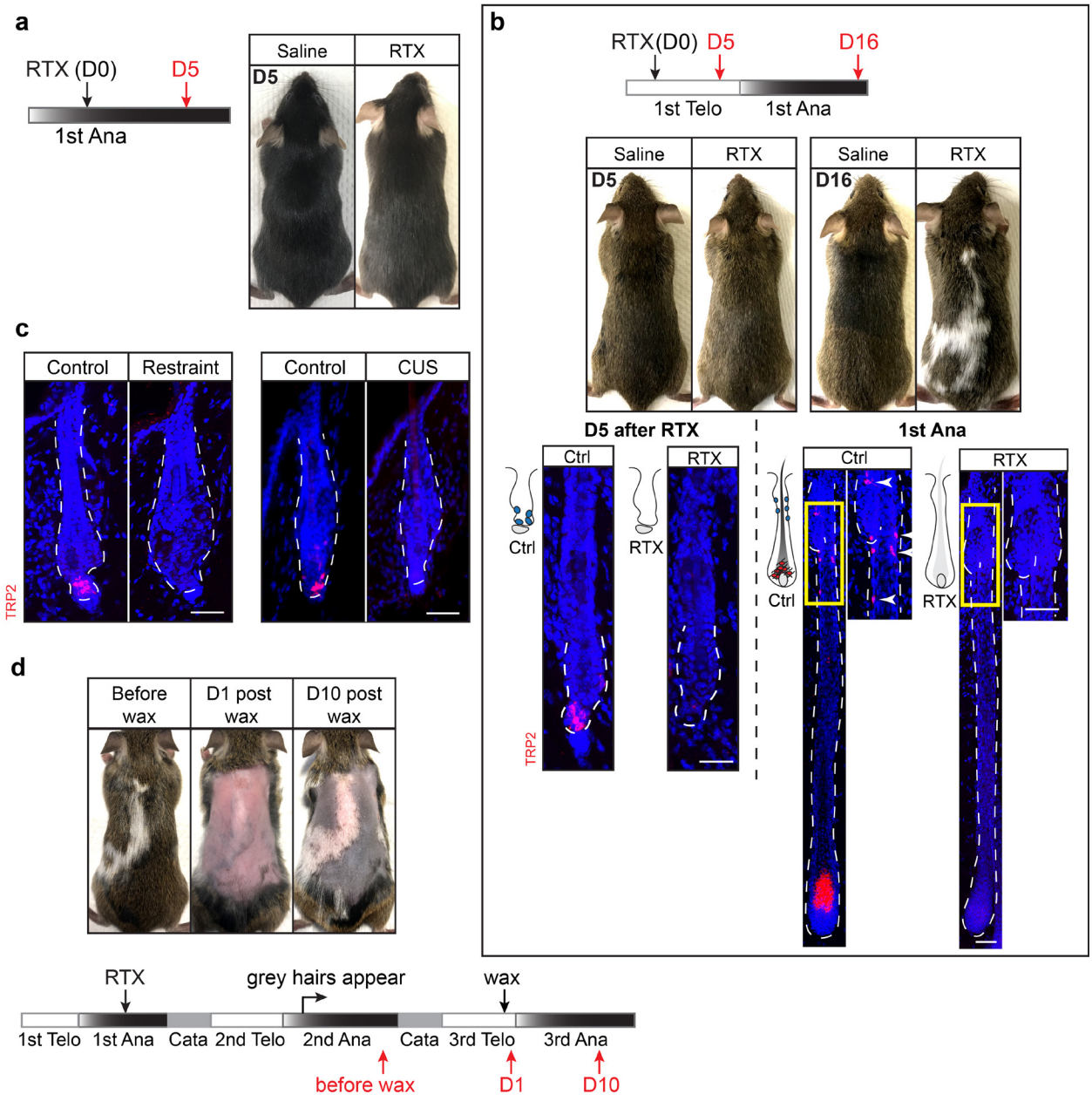

Extended Data Fig. 2 | The hair coat colour immediate after RTX injection, loss of MeSCs after RTX injection at telogen, loss of MeSCs in restraint and CUS treated mice, and permanent hair pigmentation loss in RTX injected mice. a, Hair coat colour in mice 5 days after RTX injection in anagen. RTX was injected in full anagen and the mice are examined 5 days later at late anagen. The coat colour remains black in both conditions. **b,** (Upper panel) Schematic

of experimental design for RTX injection in 1st telogen (red arrows indicate harvesting). (Lower panel) Immunofluorescent staining for TRP2 in HFs from control and RTX-injected mice (≥ 30 HFs from 4-6 mice). Yellow boxes denote the bulge region where MeSCs reside. Enlarged view of the yellow box regions are shown at the right. Arrowheads indicate MeSCs. **c,** Immunofluorescent staining of HFs for TRP2 (red) from mice subjected to chronic unpredictable stress (CUS) or restraint stress (≥ 30 HFs from 5 mice each condition). **d,** Hair coat colour is monitored in RTX-injected mice for multiple rounds of hair follicle regeneration (waxing is used to initiate new rounds of anagen). Schematic denotes the experimental design. Scale bars, 50 μm.

Extended Data Fig. 3

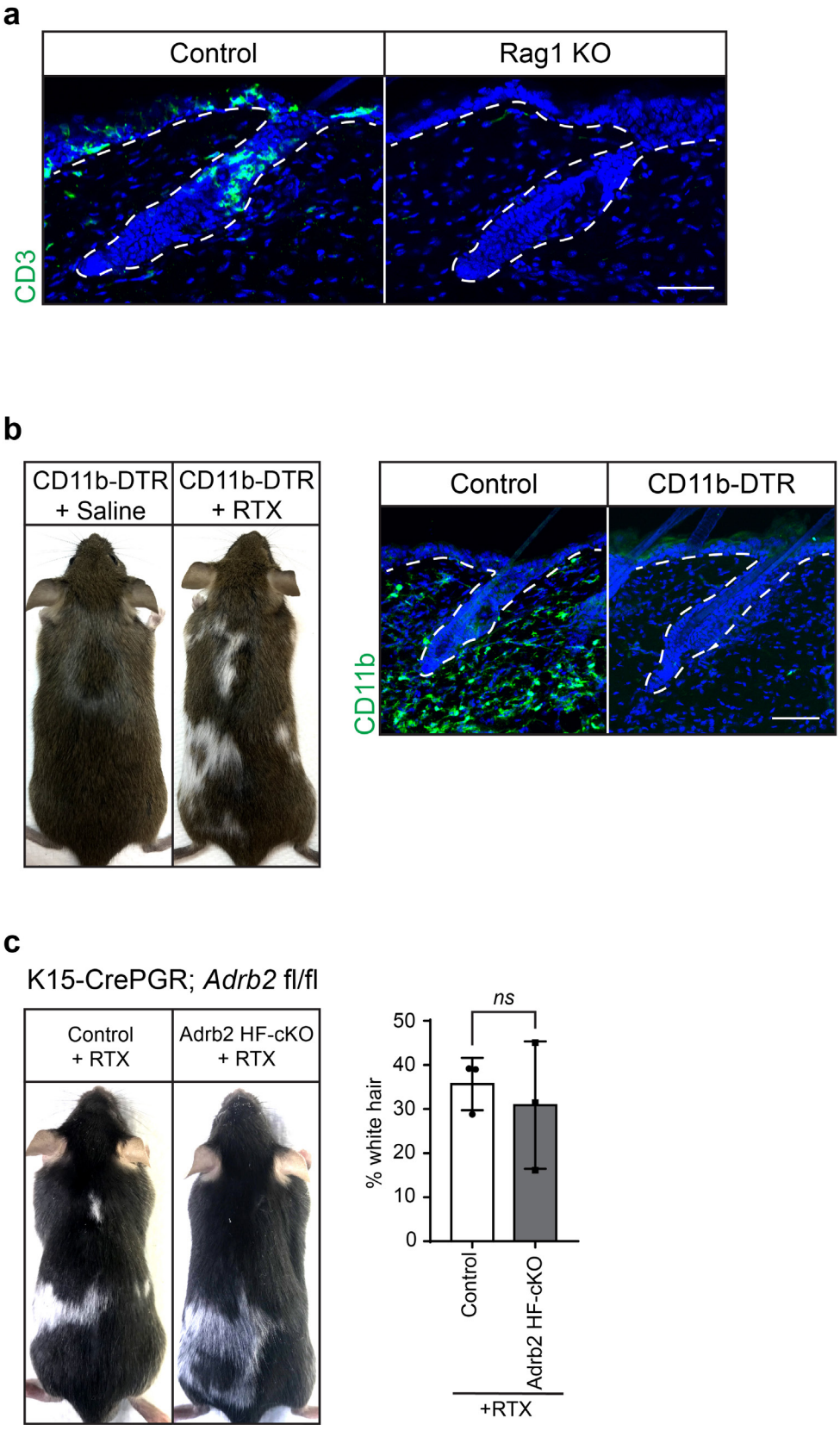

Extended Data Fig. 3 | Immune cell ablation in Rag1 KO and CD11b-DTR mice and induction of hair greying in mice with *Adrb2* cKO from HFs. a, Immunofluorescent staining of T cell marker CD3 (green) in control and Rag1 KO skin (≥ 30HFs from 4-6 mice each condition). **b,** Hair greying occurs when RTX is injected into CD11b-DTR mice treated with diphtheria toxin (DT) to deplete myeloid cells (n = 6 for each condition). Right panel: Immunofluorescent staining for CD11b (green) in DT treated control and CD11b-DTR skin (≥ 30HFs from 4-6 mice each condition). **c,** Injection of RTX into K15-CrePGR; *Adrb2* fl/fl (Adrb2 cKO) mice induces hair greying (n = 3 for each condition). Scale bars, 50 μm.

Extended Data Fig. 4

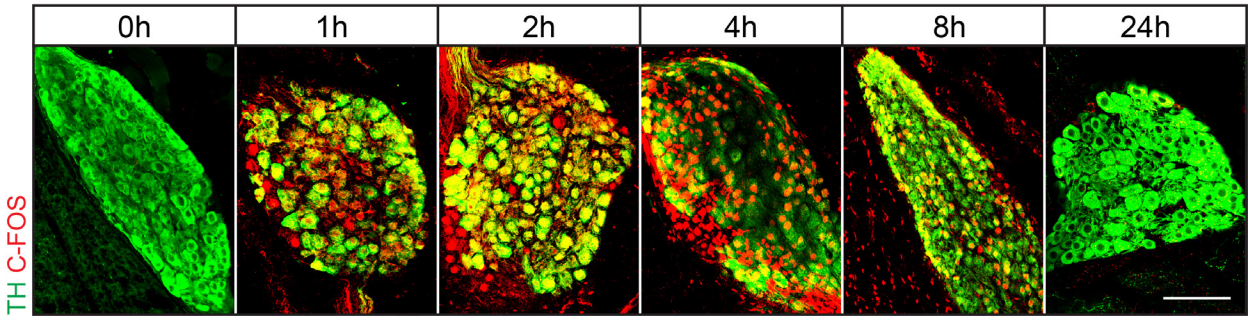

Extended Data Fig. 4 | Sympathetic nervous system induction time course after RTX injection. Immunofluorescent staining of sympathetic ganglia for TH (green) and C-FOS (red) from mice inject with RTX and harvest at different timepoints between 0 to 24 hours (≥ 10 sympathetic ganglia from 2-4 mice for each timepoints). Scale bars, 50 μm.

Extended Data Fig. 5

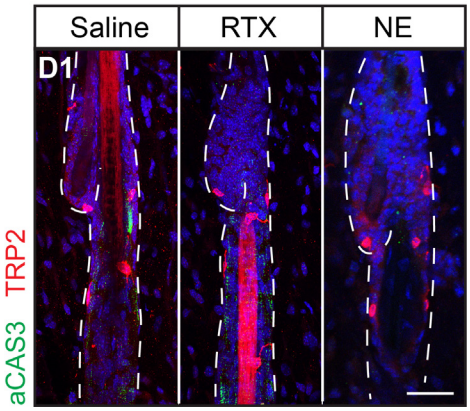

Extended Data Fig. 5 | RTX injection do not induce MeSC apoptosis shown by active-Caspase 3 (aCAS3) staining. Immunofluorescent staining of aCAS3 (green) and TRP2 (red) from mice 1 day after RTX or NE injection (≥ 30HFs from 4-6 mice for each condition). Scale bars, 50 μm.

Extended Data Fig. 6

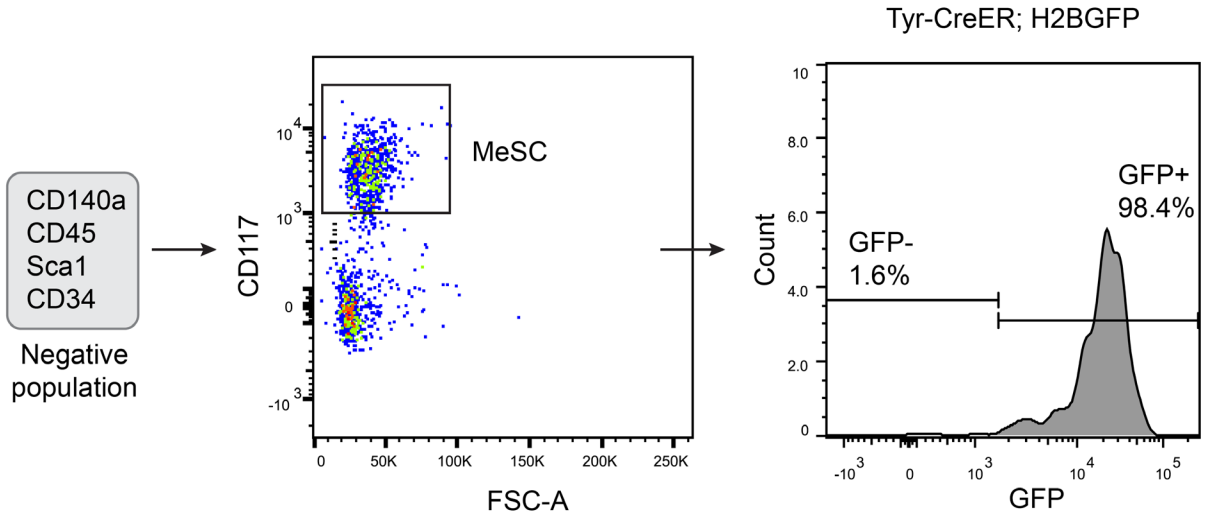

Extended Data Fig. 6 | FACS purification of MeSCs. Schematic of FACS strategy for MeSCs purification for RNAseq. MeSCs are selected based on their expression of CD117, from a population that is negative for CD140a, CD45, Sca1, and CD34.

Extended Data Fig. 7

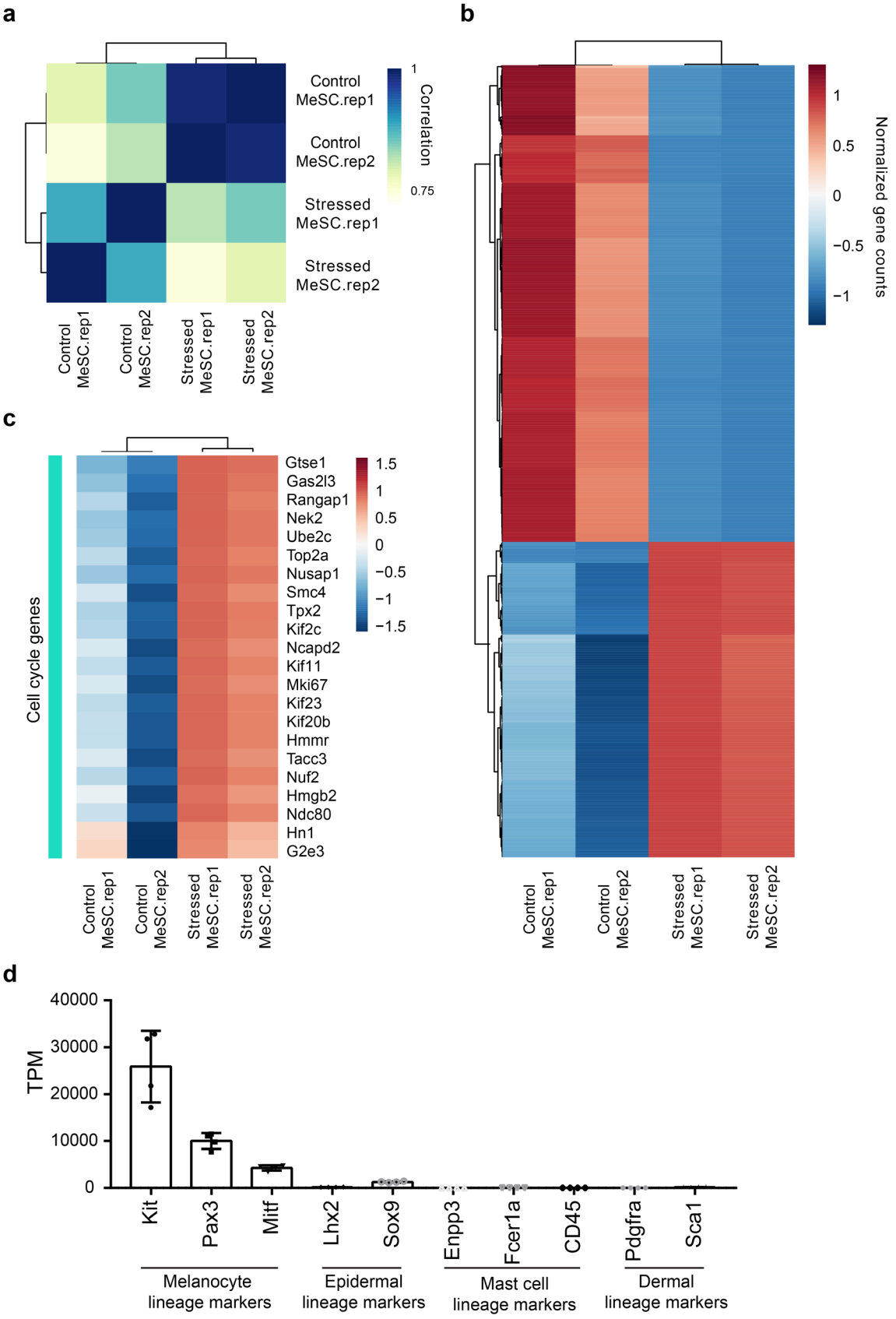

Extended Data Fig. 7 | Sample clustering analysis, clustering of differential expression genes and cell cycle signature genes, and expression of lineage marker genes in FACS purified MeSCs. a, Sample clustering based on correlation of transcriptome among control and stressed MeSCs. **b,** Heatmap of all significant differentially expressed genes (Log2FoldChange ≥ 0.58 and adjusted p value < 0.05). **c,** Heatmaps illustrating expression of cell cycle signature genes. **d,** Expression level of marker genes for different lineages in the skin confirming the purity of MeSCs used for RNAseq.

Acknowledgements

We thank G. Karsenty for Adrb2 fl/fl mice, D. Ginty for TH-CreER mice, and many colleagues who generously donated mice to JAX; C-Y Chang, Y. Fong, Q. Ma, M. Nahrendorf, A. Sarhay, and members of the Hsu lab in particular M. Gonzalez-Celeiro for discussions and comments on the manuscript, S. Kim, Y-L. Kang, and O. Chung for technical assistance; HCBI, HSCRB FACS core, histology core, FAS Small Molecule Mass Spectrometry Facility, Office of Animal Resources, and the Bauer Core Facility at Harvard University for technical support; This work was supported in part by the Smith Family Foundation Odyssey Award; the Pew Charitable Trusts; Harvard Stem Cell Institute; Harvard/MIT Basic Neuroscience Grants Program; Harvard FAS and HMS Dean's Award; American Cancer Society, NIH (R01-AR070825 and R01-AR075421 to Y.-C.H., 5R01 AR043369-23, 5R01CA222871, 5R01AR072304, 2P01 CA163222 to D.E.F. and DP2AT009499 and R01AI130019 to I.M.C.); grants from Dr. Miriam and Sheldon G. Adelson Medical Research Foundation to D.E.F.; A.R. and L.I.Z .are HHMI investigators; B.Z. was awarded with a Charles A. King Trust Postdoctoral Research Fellowship; M.H is supported by Joint Program in Molecules, Cells, and Organisms 5T32GM007598-40; Y.S. is a Helen Hay Whitney postdoctoral fellow and an awardee of the Woman in Science Weizmann Institute of Science Award; T.M.C. had a CAPES/HARVARD fellowship for visiting professor from CAPES (Process n. 88881.162285/2017-01).

Author Contributions

Designing research studies: B.Z., Y-C.H. Conducted experiments: B.Z., S.M., I.R., M.H., P.B., S.C., W.G., Y.S., E.M.F., Y.S. Intellectual contribution: Y-C.H., B.Z., S.M., Y.S., L.I.Z., A.R., J.D.B. T.M.C., I.M.C., D.E.F. Writing the manuscript: B.Z., Y-C.H., with inputs from all co-authors.

Competing Interests

Dr. Fisher has a financial interest in Soltego, Inc., a company developing SIK inhibitors for topical skin darkening treatments that might be used for a broad set of human applications. Dr. Fisher's interests were reviewed and are managed by Massachusetts General Hospital and Partners HealthCare in accordance with their conflict of interest policies.